OCS Study
MMS 2006-073

Exploratory Study of Deepwater Currents in the Gulf of Mexico

Volume I: Executive Summary

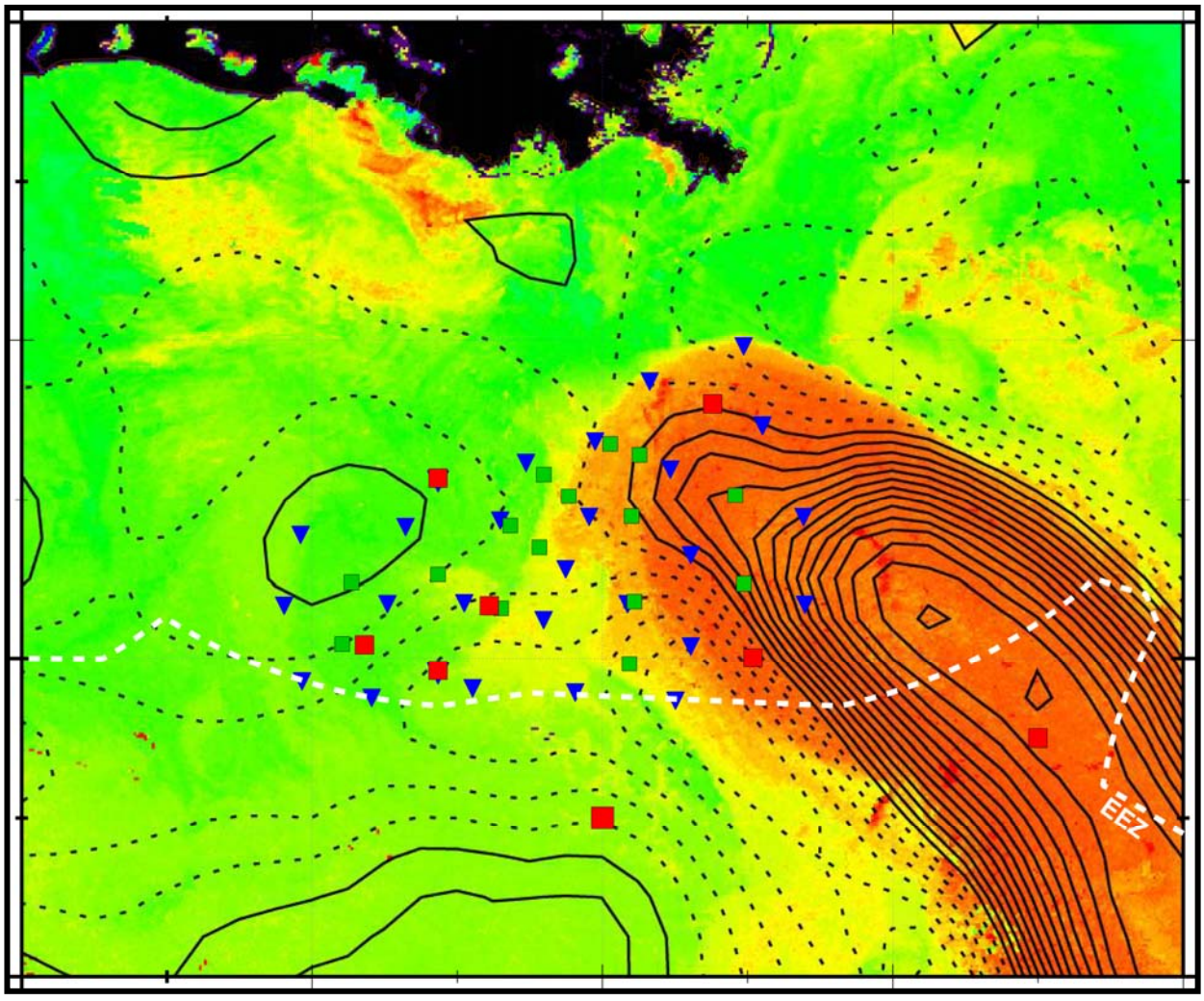

MMS U.S. Department of the Interior
Minerals Management Service
Gulf of Mexico OCS Region

OCS Study
MMS 2006-073

Exploratory Study of Deepwater Currents in the Gulf of Mexico

Volume I: Executive Summary

Authors

Kathleen Donohue
Peter Hamilton
Kevin Leaman
Robert Leben
Mark Prater
Evans Waddell
Randolph Watts

Prepared under MMS Contract
1435-01-02-CT-31152
by
Science Applications International Corporation
615 Oberlin Road, Suite 100
Raleigh, North Carolina 27605

Published by

U.S. Department of the Interior
Minerals Management Service
Gulf of Mexico OCS Region

New Orleans
December 2006

DISCLAIMER

This report was prepared under contract between the Minerals Management Service (MMS) and Science Applications International Corporation. This report has been technically reviewed by the MMS, and it has been approved for publication. Approval does not signify that the contents necessarily reflect the views and policies of the MMS, nor does mention of trade names or commercial products constitute endorsement or recommendation for use. It is, however, exempt from review and compliance with the MMS editorial standards.

REPORT AVAILABILITY

Extra copies of this report may be obtained from the Public Information Office (Mail Stop 5034) at the following address:

U.S. Department of the Interior
Minerals Management Service
Gulf of Mexico OCS Region
Public Information Office (MS 5034)
1201 Elmwood Park Blvd.
New Orleans, LA 70123-2394

Telephone: (504) 736-2519 or
1-800-200-GULF

CITATION

Donohue, K., P. Hamilton, K. Leaman, R. Leben, M. Prater, D.R.Watts, and E. Waddell. 2006. Exploratory study of deepwater currents in the Gulf of Mexico. Volume I: Executive summary. U.S. Dept. of the Interior, Minerals Management Service, Gulf of Mexico OCS Region, New Orleans, LA. OCS Study MMS 2006-073. 86 pp.

ABOUT THE COVER

Shows that portion of the northern Gulf of Mexico in which field measurements were made overlaid on a sea surface temperature image near the beginning of the field study. At that time, the warm (orange) Loop Current waters extended well into the measurement array. In this presentation, inverted triangles show the locations of PIES, green squares the locations of short or near bottom moorings and red squares are full depth mooring locations.

ACKNOWLEDGEMENT

The support and encouragement of Dr. Alexis Lugo-Fernandez, the MMS COTR, from project inception through completion has been fundamental to the program success and resulting oceanographic insights. Valuable suggestions and support from the Science Review Group (Dr. J. Bane [UNC], Dr. A. Kirwan [U. of Delaware] and Mr. D. Driver, [BP]), during the course of the study, were positive, constructive and are greatly appreciated. SAIC program personnel, Paul Blankinship (Data Management) and James Singer (Field Operations and Logistics), were crucial to the smooth data support and the outstanding data return and field activities. Mr. G. Chaplin (URI) very successfully conducted all aspects of the PIES instrumentation and field operations. GEOS provided the equipment and field personnel for deployment, rotation and recovery of most of the near-bottom moorings deployed for the study. Many additional people, too numerous to identify individually, were important to the program success, e.g., the captains and crews of the *R/V Longhorn* and the *R/V Pelican*. The patience, diligence and expertise of Mrs. Carol Harris in the production of reports is greatly appreciated by the Program Manager.

TABLE OF CONTENTS

Page

TABLE OF CONTENTS (continued)

LIST OF FIGURES

LIST OF FIGURES (continued)

LIST OF FIGURES (continued)

LIST OF TABLES

1.0 INTRODUCTION

1.1 Background

The Minerals Management Service (MMS) awarded a contract to Science Applications International Corporation (SAIC) to conduct a four-year study titled: Exploratory Study of Deepwater Current in the Gulf of Mexico (often referred to as simply the Exploratory Study). Generally, this project had been in the MMS planning phases for several years, however, the specifics were substantially affected by two years of field measurements (August 1999 – August 2001) made in the vicinity of Green Knoll (Figure 1-1) by SAIC (Hamilton et al, 2003). The objectives and background leading to the present study also incorporated the substantial insights developed as part of the MMS funded Deepwater Physical Oceanography Reanalysis and Synthesis of Historical Data conducted by Texas A&M University (Nowlin et al, 2001). In addition to the Exploratory Study, the MMS is presently funding two additional field measurement programs with the goal of an improved documentation and understanding of physical oceanographic conditions in the deepwater of the northern GOM. The Study of Deepwater Currents in the Western Gulf of Mexico and the Study of Deepwater Currents in the Eastern Gulf of Mexico, while not concurrent with the Exploratory Study these projects will provide valuable insights to conditions in these areas of the US EEZ that bracket the present study area. Note that the Western GOM has two coordinated components producing measurements within the America and the Mexican EEZs.

The specified domain for field measurements for the Exploratory Study is shown in Figure 1-1. The east-west extent was from 88°W to 94°W, and the north-south extent was defined by the 1,000 m isobath in the north and the EEZ boundary on the south. The field measurement program designed and implemented by SAIC and its team of scientists fully supported the goal and requirements specified in the Request for Proposal (RFP).

The Exploratory Study field measurement program as called for in the RFP and designed by SAIC's team had three primary objectives:

A. Increase deepwater current database and knowledge of the deep circulation in the Gulf of Mexico (GOM),

B. Measurements sufficient to estimate parameters needed to design full-scale PO studies in deepwater regions of the GOM, and

C. Collect current data sufficient to test and/or evaluate the hypotheses listed below:

- **H1**: Currents shallower than 800 m are dynamically uncoupled from currents at depths greater than about 1,000 m.
- **H2**: Rare mid-water jets occur in areas of eddy-eddy interactions.
- **H3**: Currents in water depths greater than 1,000 m never show a large vertical gradient of velocity.

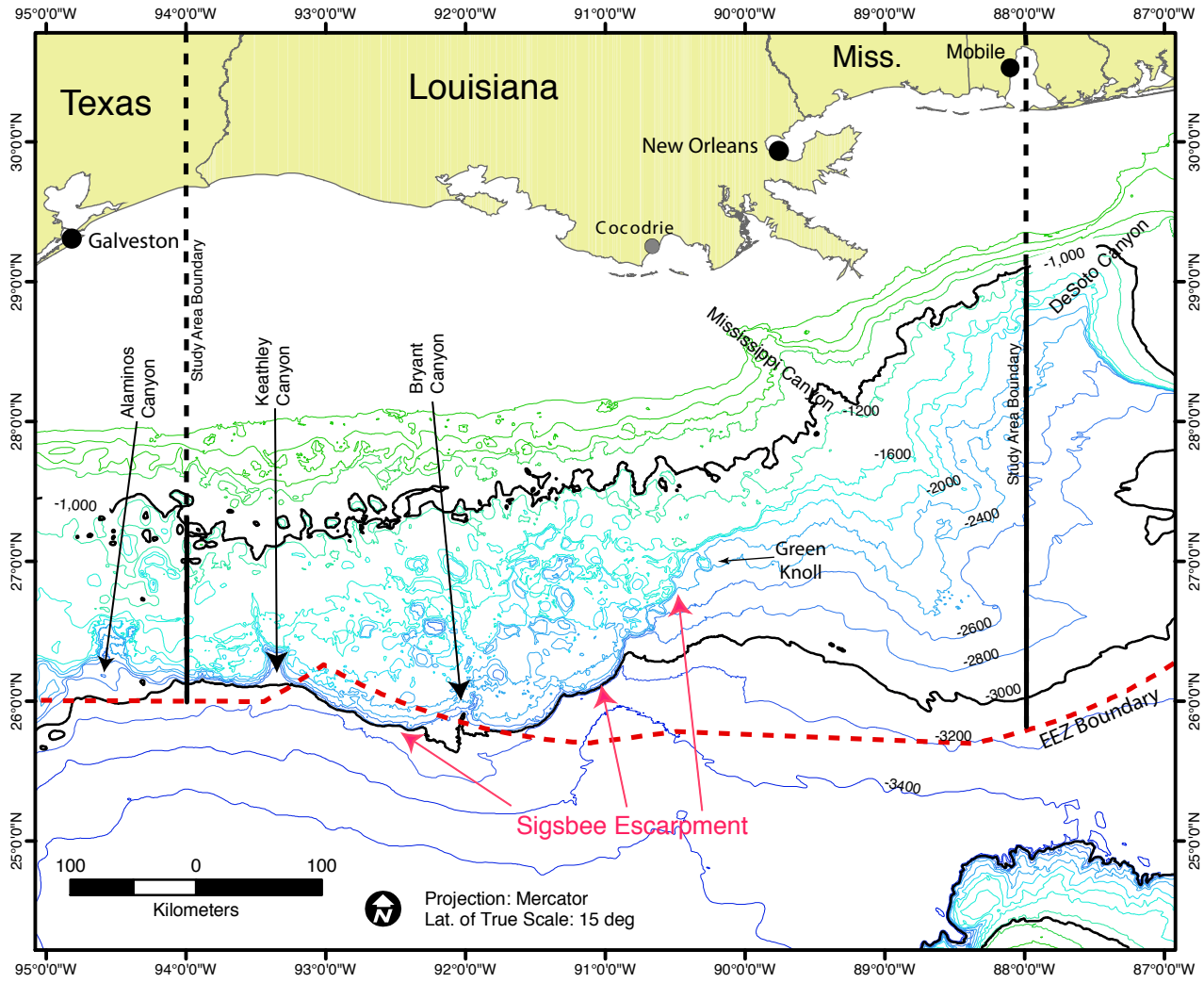

Figure 1-1. Map showing locations of key bathymetric features and several place names to orient the reader to the extent of the study area and bottom features that may be important to discussions of deep water currents.

H4: Deepwater parameters measured in areas dominated by cyclones/anticyclones of scales of 50-100 km are not different from areas not dominated by cyclones/anticyclones of 50-100 km.

H5: There are no differences in the occurrence and/or intensity of near bottom currents near steep bathymetric gradients and areas of small bathymetric gradients**.**

H6: The characteristics of topographic Rossby waves change from east to west in the Gulf of Mexico because of changes in bottom slopes and frictional dissipation that causes the TRW's to reflect, trap and dissipate by wave breaking**.**

H7: Circulation below 1,000 m in the Gulf of Mexico is dominated by cyclone/anticyclone pairs and is fundamentally cyclonic.

H8: Storm generated inertial oscillations trigger resonant phenomena that propagates into deepwater.

1.2 Proposed Approach

The SAIC team of scientists and engineers designed an innovative, data rich, and observationally integrated field measurement program that supported all of the program objectives. This was done using: Inverted Echo Sounders with Pressure (PIES), direct and acoustic current velocity measurements with related hydrographic variables, Lagrangian drifters and remote sensing. As proposed, PIES in conjunction with conventional current meter moorings provided the following key cost-effective design advantages:

- Full-depth current profiles at sixteen sites over the study area (See PIES locations relative to Tall and Short Mooring locations in Figure 1-2).

- Substantially broader and better resolved time varying, 3-D coverage of the temperature and salinity structure than was possible with 15 conventional moorings.

- Bottom pressure measurements at 25 PIES sites to map deep eddies and distinguish between deep eddies and topographic Rossby waves (TRW).

- An analytical method for determining the baroclinic and barotropic bottom pressure contributions to altimeter measurements of sea surface height (SSH).

Proposed Study Area

As presented in Figure 1-1, the Sigsbee Escarpment is a major bathymetric feature affecting conditions and processes in the study area. As shown, the Escarpment is oriented approximately NE to SW from approximately 89°W to 92°W. Generally, the relative elevation change across the Escarpment (top to base) is on the order of 500 m. However, the Escarpment is inclined such that the top of the Escarpment is approximately 1500 m below the surface at the NE end and approximately 2500 m on the SW end as shown in Figure 1-1. On the eastern end of the study area a more gently sloping bottom occurs between the 2,000 and 3,000 m isobaths. The location and presence of this latter area may be of importance in discussions of the characteristics and behavior of topographic rossby waves (TRW).

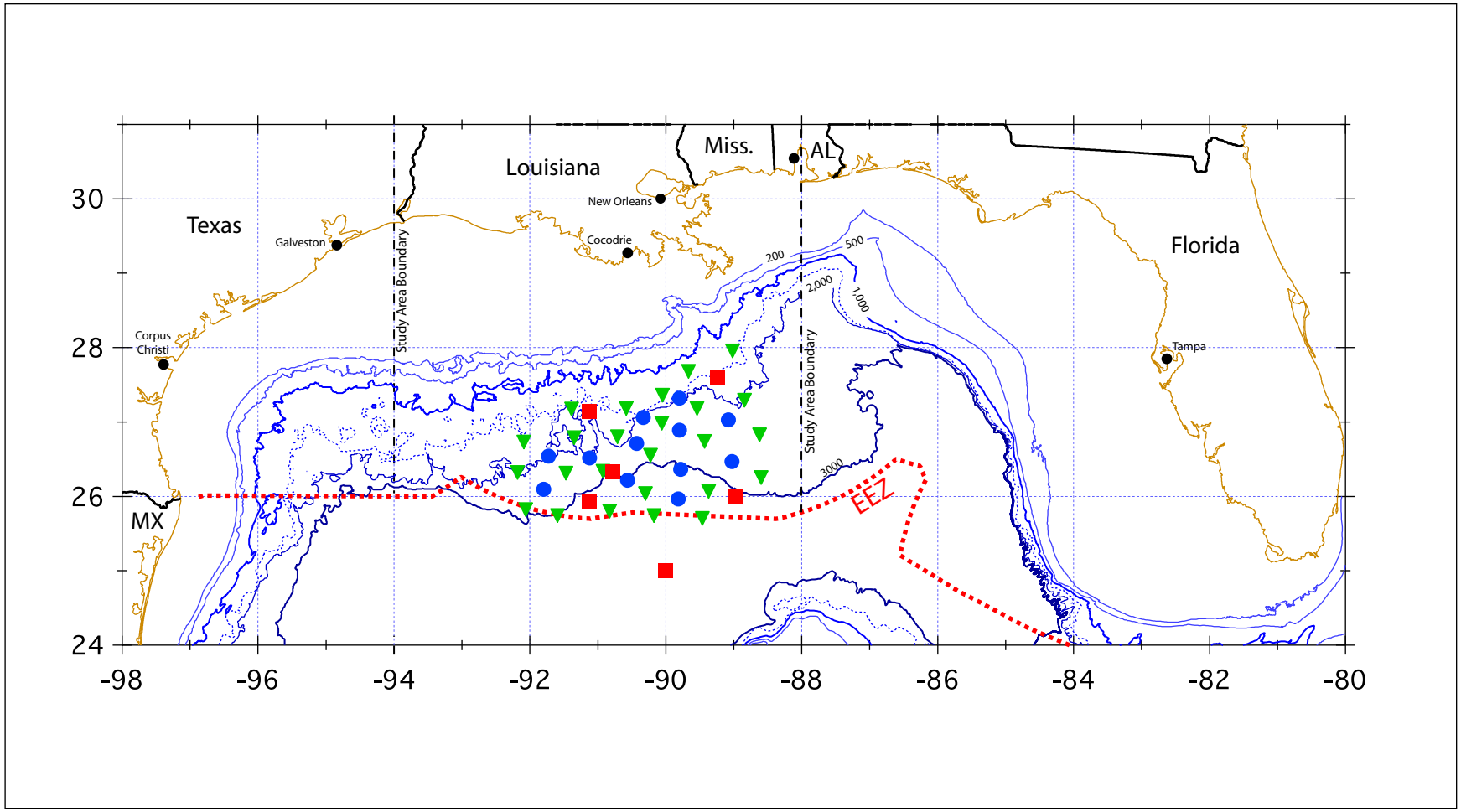

Figure 1-2. Map showing the regional bathymetry of the northern GOM, the east-west and north-sourth extent of the study area. In the above map, the locations of PIES are indicated by inverted triangles, the near-bottom or short moorings by blue solid circles and the full depth moorings (Exploratory, LSU and CICESE) are shown by red solid squares.

By coordinating other programs that were completely or partially funded by the MMS, the Exploratory Study had access to measurements taken over an area larger than the spatial extent defined in Section 1.1. Particularly, Louisiana State University deployed a well-instrumented, full-depth mooring within the Exploratory Study domain. Additionally, the MMS supported CICESE to instrument and deploy a full-depth mooring south of the Exploratory Study area and within the Mexican EEZ. Data sharing among the various entities responsible for acquiring the field measurements was such that each participant (LSU, CICESE and the Exploratory Study) had access to the complete set of observations regardless of the origin. This sharing arrangement has been well defined by the MMS data-sharing protocols.

1.3 Team Participants

Presented below are Science Team/Principal Investigators (PI) that contributed to the analyses and subsequent writing of this report. Also shown are the primary SAIC personnel that supported the project. Note that each PIs was supported in their various activities by scientists and engineers at their home institutions. These additional support personnel were essential to the success of all aspects of the study from observations to analyses to graphics production.

Science Team and associated measurement responsibility:

PIES

Dr. Kathleen Donohue, University of Rhode Island
Dr. Randolph Watts, University of Rhode Island

Lagrangian

Dr. Kevin Leaman, University of Miami
Dr. Mark Prater, University of Rhode Island

Remote Sensing

Dr. Robert Leben, University of Colorado

In-situ Current Measurements

Dr. Peter Hamilton, SAIC

It is important to note that the complete and comprehensive data set was available to each of the members of the Science Team, thus, a multivariate approach was used by each scientist. In conjunction with this approach, there was considerable collegial interaction so that combined expertise was brought to bear on the complex processes occurring in the upper and lower layers of the water column in the study area.

The Science Team was supported by the Management and Logistics personnel as follows:

Dr. Evans Waddell, Program Manager
Mr. James Singer, Logistics Manager and Cruise Chief Scientist
Mr. Paul Blankinship, Data Manager.

Twelve of the near-bottom moorings were built, deployed and recovered by GEOS. Mr. David Szabo was the primary point of contact for most of the study in support of this component of the field measurements. All other moored current meter arrays were the responsibility of SAIC. URI was responsible for all aspect of the PIES instrumentation, including building, preparation, deployment and recovery.

1.4 Technical Report Organization

This report provides a dynamic characterization of processes occurring in the upper and lower layers of the north central GOM. In support of this goal, report chapters include:

- Chapter 1: Introduction that describes the general context and content of the study.
- Chapter 2: Experimental Design and Methodology that briefly describes measurements made and associated aspects of the study.
- Chapter 3: Gulf-wide and Historical Perspective that provides information to the reader on some of the work done previously as well as metrics and descriptions of dynamic features that affect the study area directly or indirectly.
- Chapter 4: Basic Description in the Study Area provides a general characterization of the basic conditions and processes occurring in the study area.
- Chapter 5: Interpretation and Analyses provides a more in-depth presentation of the results of analyses in both the upper and lower layer of the water column.
- Chapter 6: Upper and Lower Layer Interactions describes possible linkages that may relate conditions in the upper and lower layers of the water column.
- Chapter 7: High-frequency Oscillations describes the measured current variations that occurred at or above the tidal or inertial frequency with a tentative explanation for some of the episodes documented.
- Chapter 8: Summary and Recommendation provides a brief review of key understandings developed during this study in conjunction with suggestions for future studies.

The main chapters of the Technical Report are followed by a series of Appendices. These contain information that the reader may find of use, but if it had been included in the main body of the report would have tended to detract from a focus on the insights to conditions and processes resulting to date from the measurements and analyses associated with the Exploratory Study.

2.0 EXPERIMENT DESIGN AND METHODOLOGY

2.1 Currents

In keeping with the objectives of the Exploratory Study an array of moorings supporting a variety of instruments were deployed at the end of February 2003 and recovered in the middle of April 2004. Vertical and horizontal instrument placement was designed to resolve scales of motion and to provide essential reference level velocities for use in conjunction with geostrophic current profiles developed from PIES observations. As proposed and implemented, two types of mooring were deployed: Tall or full-depth moorings (4) and short or near-bottom moorings (15) (see Figure 2-1). There was consistent instrument placement on these moorings relative to the water surface for the tall moorings and relative to the local bottom for the short moorings The tall moorings also had a variety of sensors for measuring temperature, salinity and pressure (T/C/P). The placement of these instruments and the current meters are summarized in Table 2-1. The overall data return for the Exploratory Study instrumentation was 97.5%.

Table 2-1

Moored instrument measurement levels for the Exploratory Study.
(Initial Deployment with nominal instrument depths)

Mooring	Water Depth (M)	Instrument Depth (M) (MAB)	Instrument Type (SN)
L1	1512	75	C/T/D (0057)
		150	C/T/D (1719) (2702)
		225	C/T/D (2693) (2703)
		300	TEMP (C919)
		400	ADCP (75 KHz) – up (924)
		500	TEMP (C937)
		600	TEMP (C929)
		750	S4 (07801745)
		1000 (500)	RCM-7/8(6922) (7528)
		1400 (100)	RCM-7 (9948)/MK2 (457)
L2	1762	75	C/T/D (0059)
		150	C/T/D (1720) (2701)
		225	C/T/D (2694)
		300	TEMP (C933)
		400	ADCP (75 KHz) – up (1495)
		402	T/D (4660)
		500	TEMP (C940)
		600	TEMP (C959)
		750	S4 (08161753)
		751	T/D (Deployment 2 only) (4663)
		1000	RCM-8 (7582) (12788)

Table 2-1 Moored instrument measurement levels for the Exploratory Study. (Initial Deployment with nominal instrument depths) (continued)

Mooring	Water Depth (M)	Instrument Depth (M) (MAB)	Instrument Type (SN)
L2 (cont'd)	1762 (cont'd)	1400 (350) 1650 (100)	RCM-7 (9949)/MK2 (453) RCM-8 (12803)
L3	2998	75 150 225 300 400 402 500 600 750 1000 1500 2000 2500 (500) 2900 (100)	C/T/D (2695) C/T/D (2696) C/T/D (2697) TEMP (C939) ADCP (75 KHz) – up (1607) T/D (4662) TEMP (C960) TEMP (C947) RCM-7 (10350)/S4 (08161757) RCM-7 (6892) (9525) RCM-8 (7528) (12789) RCM-8 (12808) RCM-8 (12809) RCM-8 (12810)
L4	3350	75 150 225 300 400 402 500 600 750 1000 1500 2000 2500 2900 (450) 3250 (100)	C/T/D (2698) C/T/D (2699) C/T/D (2700) TEMP (C944) ADCP (75 KHz) – up (1536) T/D (4661) TEMP (C946) TEMP (C943) RCM-7 (9524)/S4 (08161755) RCM-7 (10881) RCM-8 (10533) (9524) RCM-8 (12804) RCM-8 (12805) RCM-8 (12806) RCM-8 (12807)
M1	1981	1481 (500) 1881 (100)	RCM-7 (12391) RCM-7 (12415)
M2	2326	1826 (500) 2226 (100)	RCM-7 (12403) RCM-8 (12480)
M3	1740	1640 (100)	RCM-8 (7356)
M4	1335	1235 (100)	RCM-8 (7357)
M5	1304	1204 (100)	RCM-8 (9268)

Table 2-1 Moored instrument measurement levels for the Exploratory Study. (Initial Deployment with nominal instrument depths) (continued)

Mooring	Water Depth (M)	Instrument Depth (M) (MAB)	Instrument Type (SN)
M5 (cont'd)	1304 (cont'd)	1819 (500) 2219 (100)	RCM-7 (12134) (10621) RCM-8 (5721)
N3	2580	2080 (500) 2480 (100)	RCM-8 (12477) RCM-8 (12110)
N4	2538	2038 (500) 2438 (100)	RCM-8 (12475) (12473) RCM-8 (6238)
N5 N5	2020	1520 (500) 1920 (100)	RCM-7 (12398) RCM-7 (12429)
N6	2332	1832 (500) 2232 (100)	RCM-7 (12278) RCM-8 (12050)
O1	2830	2330 (500) 2730 (100)	RCM-8 (11574) RCM-8 (11258)
O2	3018	2518 (500) 2918 (100)	RCM-8 (11263) RCM-8 (11257)
O3	2960	2460 (500) 2860 (100)	RCM-8 (12049) RCM-8 (11492) (11512)
O4	2222	1722 (500) 2122 (100)	RCM-7 (12414) RCM-8 (11577)
Q2	3211	2711 (500) 3111 (100)	RCM-8 (12474) RCM-8 (12111)

The Exploratory observations were supplemented with measurements made on full-depth moorings deployed by LSU (Mooring L5 in Figure 2-1) and CICESE (Mooring L6 in Figure 2-1). Additionally, the MMS and the Deepstar Consortium agreed on a data exchange by which current observations made on near-bottom moorings would be available for use in the analysis and interpretation phase of the Exploratory Study. Each of these six (S1-S6 on Figure 2-1) moorings had current meters 3 above the local bottom at locations across the Sigsbee Escarpment on 91°W starting just north of full-depth mooring L4. For the present study these are collectively referred to as SEBSEP moorings.

2.2 LaGrangian Measurements

2.2.1 RAFOS Float Methodology

RAFOS floats (Rossby et al, 1986) are neutrally buoyant glass-tube floats that can be ballasted in the laboratory to drift with the currents below the surface at a user-selected pressure (roughly, depth) or density for extended periods. The floats are equipped with temperature and pressure sensors and with an acoustic hydrophone that listens to the arrival times of acoustic signals sent from sound sources deployed in the ocean. Floats were programmed to record acoustic travel

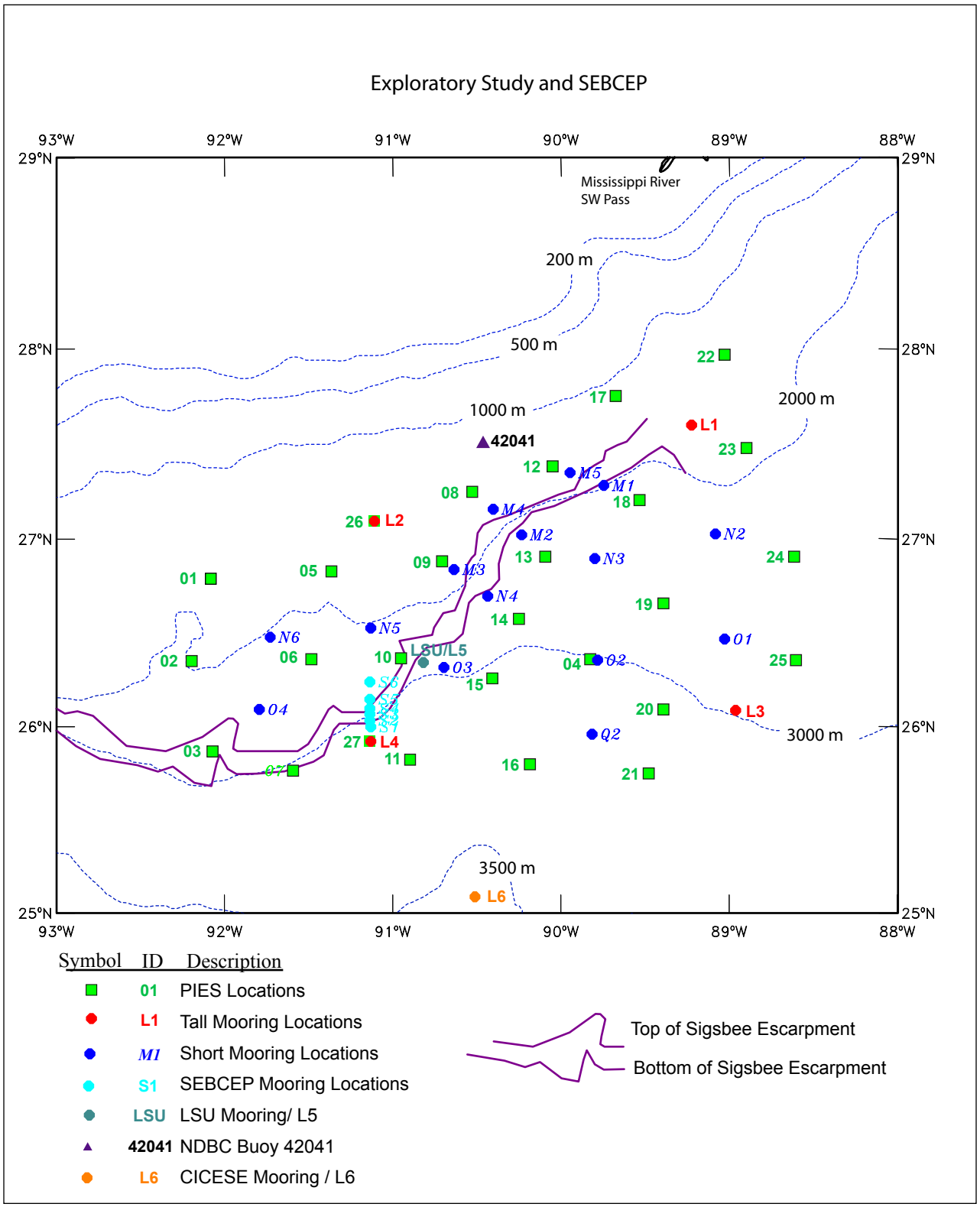

Figure 2-1. General bathymetric map showing the location of various instrument sites used during the Exploratory Study. The legend at the bottom indicates the relation of map symbols to the types of measurements made.

time and the other data every eight hours. At the end of the deployment (one year for the initial 30 floats) the floats dropped a ballast weight, surfaced, and transmitted all their accumulated data to shore via satellite (Service Argos). Since our focus was on deep (below 1000 m) currents, all floats were ballasted to follow pressure as opposed to density surfaces.

2.2.2 PALFOS Float Methodology

PALFOS floats are PALACE- or APEX-type profiling floats (Davis et al, 2001) with the added capability to be tracked acoustically in much the same manner as RAFOS floats. The six PALFOS floats in this experiment were ballasted to drift at a "rest depth" of 1000 m between profiles. Every ten days these floats were programmed to surface and transmit the acoustic tracking data (arrival times of acoustic signals from the sources) to shore via Service Argos. When the floats surfaced they would also obtain a CTD (conductivity/temperature/depth) profile using a SeaBird CTD sensor. These data would also be transmitted to shore via Argos and would allow the determination of important hydrographic quantities, such as potential density.

Sound sources were deployed at three locations in the eastern, central and western GOM to provide navigating triangulation for all floats. These sources provided three float positions per day. In addition, an acoustic monitor or ALS was deployed on a full depth mooring to track possible changes in the clocks aboard the sound sources. Unfortunately, two of the sources (SoSo2, SoSo3) failed approximately two months after the start of the experiment in April 2003 and were replaced in October 2003 by sources kindly loaned to the project by the Institut fur Meereskunde in Germany (Drs. Walter Zenk and Fritz Schott).

2.3 PIES

A mesoscale-resolving array of twenty-seven inverted echo sounders with pressure gauges (PIES) were deployed March 2003 and recovered in April 2004 (Figure 2-1). The PIES is a bottom-mounted instrument that emits 12 kHz sound pulses and measures the round trip travel times or τ (tau) of these acoustic pulses from sea floor to sea surface and back. The PIES, equipped with a pressure gauge, also measures bottom pressure. A detailed description of instrument and initial processing may be found in Hamilton et al. (2003).

The broad extent of the array, nominally 92°W to 88°W, 26°N to 28°N enabled a quantitative mapping of the regional circulation. Round-trip acoustic travel allowed estimation of vertical profiles of temperature, salinity, and density, utilizing empirical relationships established from historical hydrography. Pressure was leveled via geostrophy using mean current measurements. Deep pressure records combined with estimated horizontal density gradients yielded referenced geostrophic velocities. With this array we produced 4-D maps (x,y,z,t) of temperature, salinity, density, and velocity. Figure 2-2 illustrates the various views of current and temperature structure provided by the PIES and deep current meter mooring array for August 31, 2003.

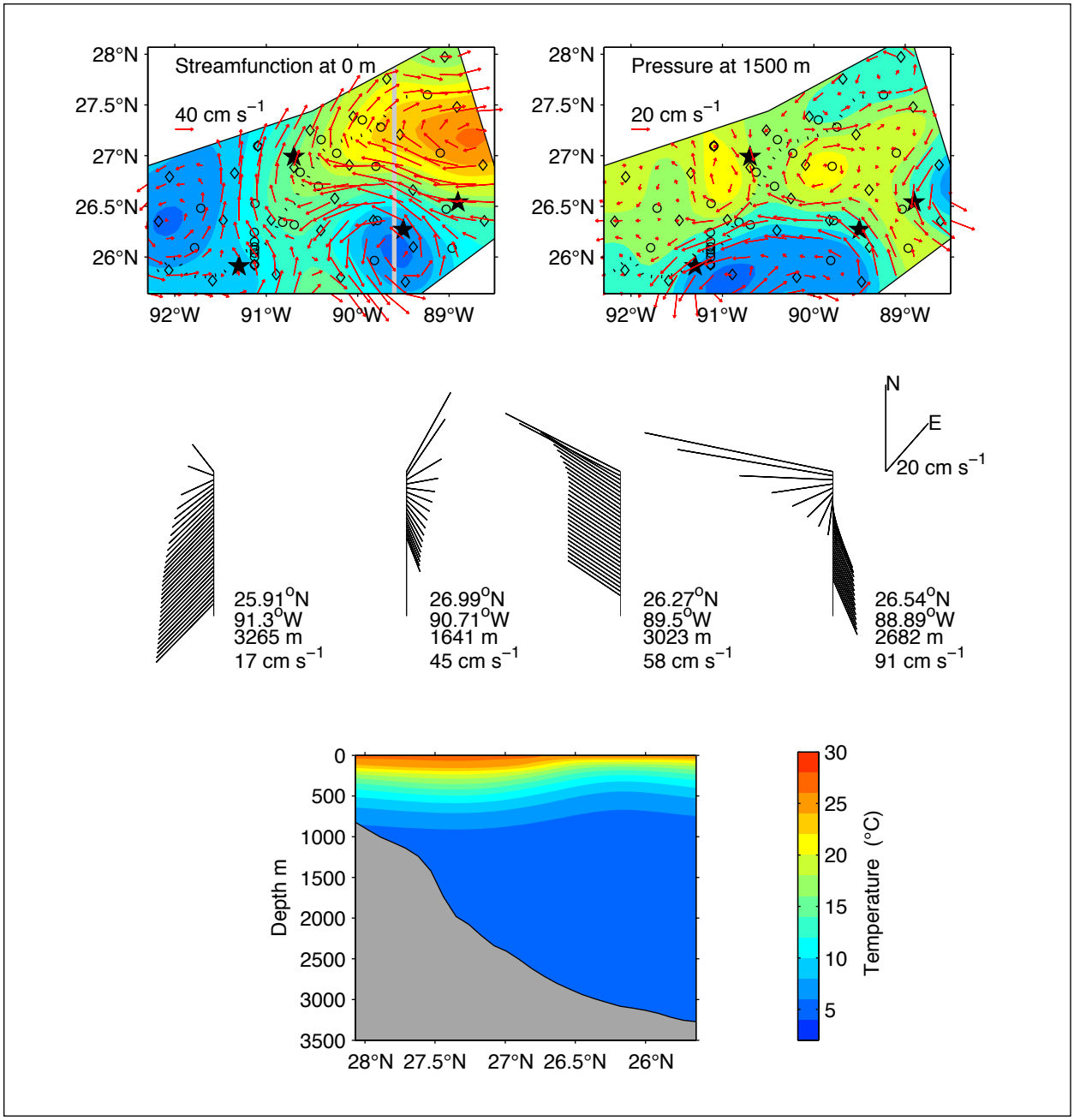

Figure 2-2. Several views of current and temperature structure in the region for August 31, 2003 provided by the PIES and deep current measurements. Top panels: Streamfunction at the sea surface (left) and pressure at 1500 m (right) in plan view. Contour intervals are 5 km m s^{-1} and 0.02 dbar, respectively. Anticyclonic circulations are shown by reddish hues; cyclonic circulations by bluish hues. Currents vectors plotted at 20 km spacing. PIES sites denoted by the diamonds; current meter moorings indicated by the circles. A dotted line marks the center of the Sigsbee escarpment. Middle panels: Vector profiles of absolute velocity every 100 m from the surface to the bottom at 4 locations indicated by the solid black stars in top panels. Latitude, longitude, bottom depth, and surface speed at each location are noted. Bottom panel: Cross-section of temperature in °C along the gray line in the top left panel.

2.4 Remote Sensing

The remote sensing component of the Exploratory Study was designed to acquire satellite data to aid in the interpretation of mesoscale features and physical data in the study area. A combination of a variety of satellite platforms have been used.

To carry out this task, the Colorado Center for Astrodynamic Research (CCAR) collected and processed a complementary suite of satellite observations from satellite altimeter and radiometer remote sensing data systems. This suite incorporated sea surface height (SSH) data with high-resolution sea surface temperature (SST) and ocean color imagery. Satellite altimetry provided the all-weather multi-satellite monitoring capability required to map mesoscale circulation variability in the GOM. During cloud free conditions, multi-channel radiometry was used to supplement the altimetric sampling by providing high-resolution synoptic imagery for monitoring the LC front and rapidly evolving small-scale eddies in and around the study region.

Altimeter data used during the Exploratory Study were the near real-time and archival data streams available from TOPEX/Poseidon (T/P), ERS-2, Geosat Follow-on, Jason-1 and Envisat satellite missions. Processing of the SSH data was based on near real-time mesoscale analysis techniques designed to exploit the multi-satellite altimetric sampling (Leben et al., 2002). This method has been used to monitor the GOM operationally since November 1995. Altimeter data from a total of five satellites were available during the program time period. PIES and satellite altimetry are complementary data types. Although the two measurement systems measure completely different physical quantities, they both yield an estimate of the height of the ocean surface relative to a datum.

3.0 GULFWIDE AND HISTORICAL PERSPECTIVE

3.1 Upper Ocean Circulation

The LC dominates upper ocean circulation in the eastern and central GOM, therefore, no description of observations in the Exploratory Study region is complete without accounting for the position and movement of the LC and associated eddies. In this section, an historical perspective is used to place Gulfwide, upper-ocean circulation documented during the Exploratory Study in the context of expected or "typical" conditions. Continuous altimeter mapping of the SSH in the GOM since 1993 provides the basis for such an historical perspective. Using available time series, the position of the LC and individual LC eddies from 1 January 1993 through 1 July 2004 can be compared with similar estimates from the Exploratory Study interval of 1 April 2003 through 31 March 2004.

3.1.1 Historical Perspective

From altimetry, an 11.5-year time series of LC maximum extension and length are shown in Figure 3-1 and area, volume, and circulation in Figure 3-2 with the time period spanning the Exploratory Study Program highlighted in black. Histograms of each metric are shown in the lower panels of each of the figures. Overlaying histograms of the longer interval with the present study interval show different distributions, as might be expected. It is surprising how similar the mean LC metric values are for the long and short intervals. The spatial structure of the mean LC position as determined by the 17-cm tracking contour is also nearly identical in the mean SSH height fields computed by averaging the daily SSH maps over the 1-year program time period and by averaging over the entire 11.5-year altimeter record (Figure 3-3). This agreement between the mean LC metric values and mean SSH fields from a single year versus the entire 11.5-year time period reflects the nearly stationary behavior exhibited by the LC. This stationarity is also supported by the good agreement between the altimetry derived statistics and those developed using remotely sensed data prior to routine availability of altimetry (Hamilton et al., (2000) and Leben (2005)).

3.1.2 Loop Current Eddies

Sixteen LC eddy separation events were identified in the 11.5-year altimeter record, which includes the Exploratory Study. The separation date, separation period, eddy name and eddy area at the time of separation are tabulated for each of the 16 observed events in Table 3-1. All but one separation events were identified using the SSH 17-cm tracking contour.

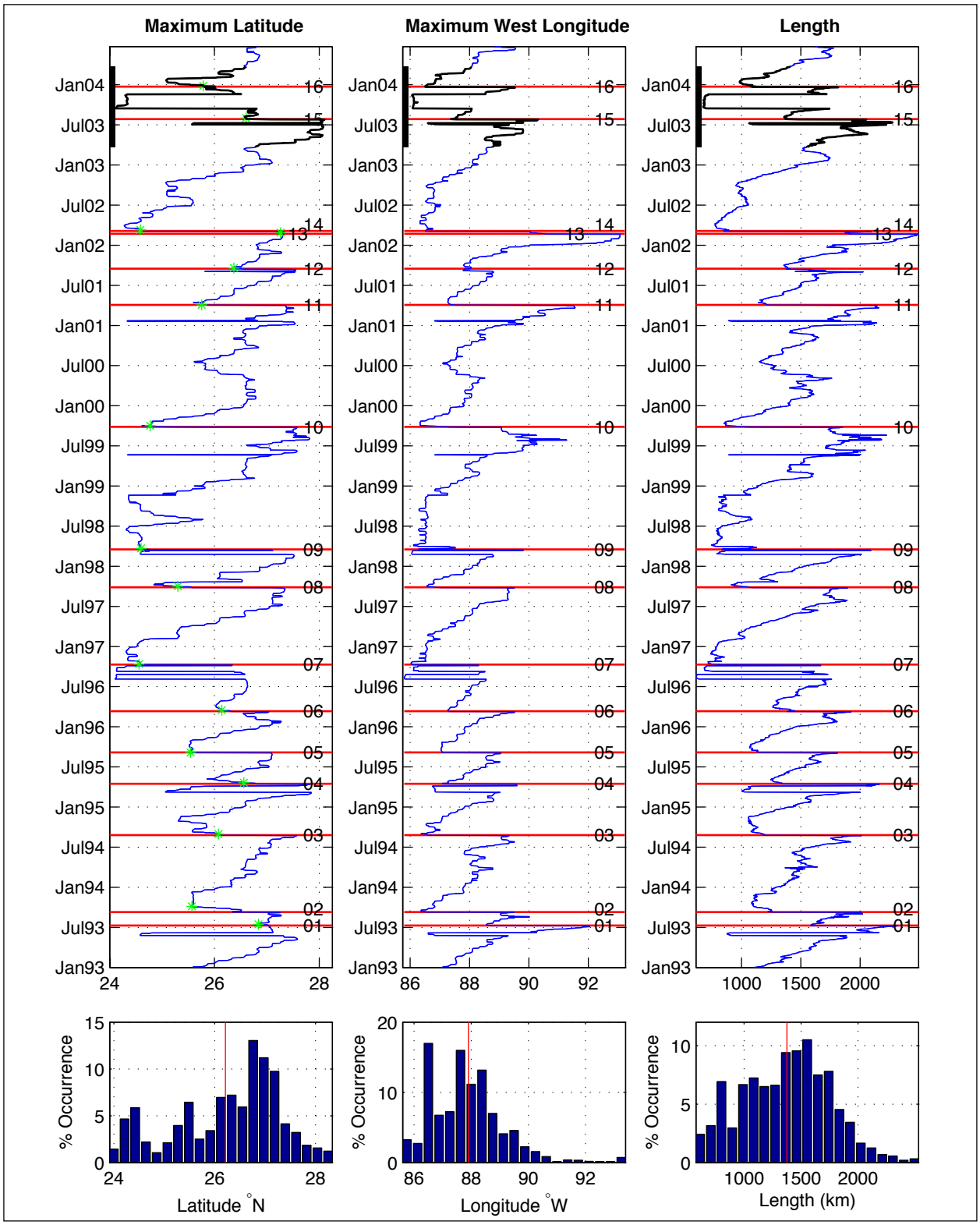

Figure 3-1. Loop Current maximum northern/western extension and length time series with percent occurrence histograms. The horizontal red lines identify the 16 LC eddy separation events and vertical red lines are the mean of the time series. Green stars identify the LC maximum latitude just after separation.

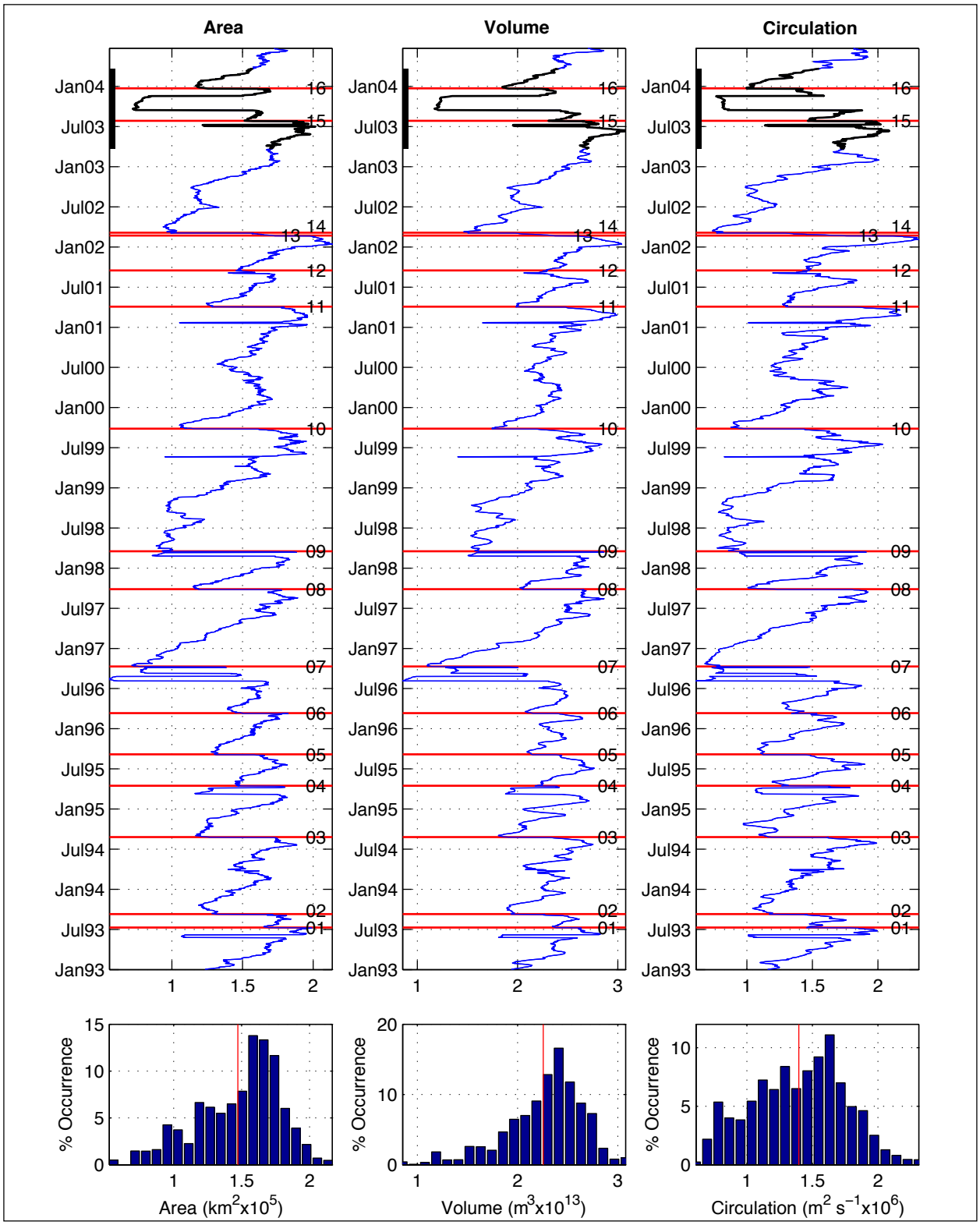

Figure 3-2. Loop Current area, volume and circulation time series with percent occurrence histograms. The horizontal red lines identify the 16 LC eddy separation events and vertical red lines are the mean of the time series. The Exploratory Study time period is highlighted.

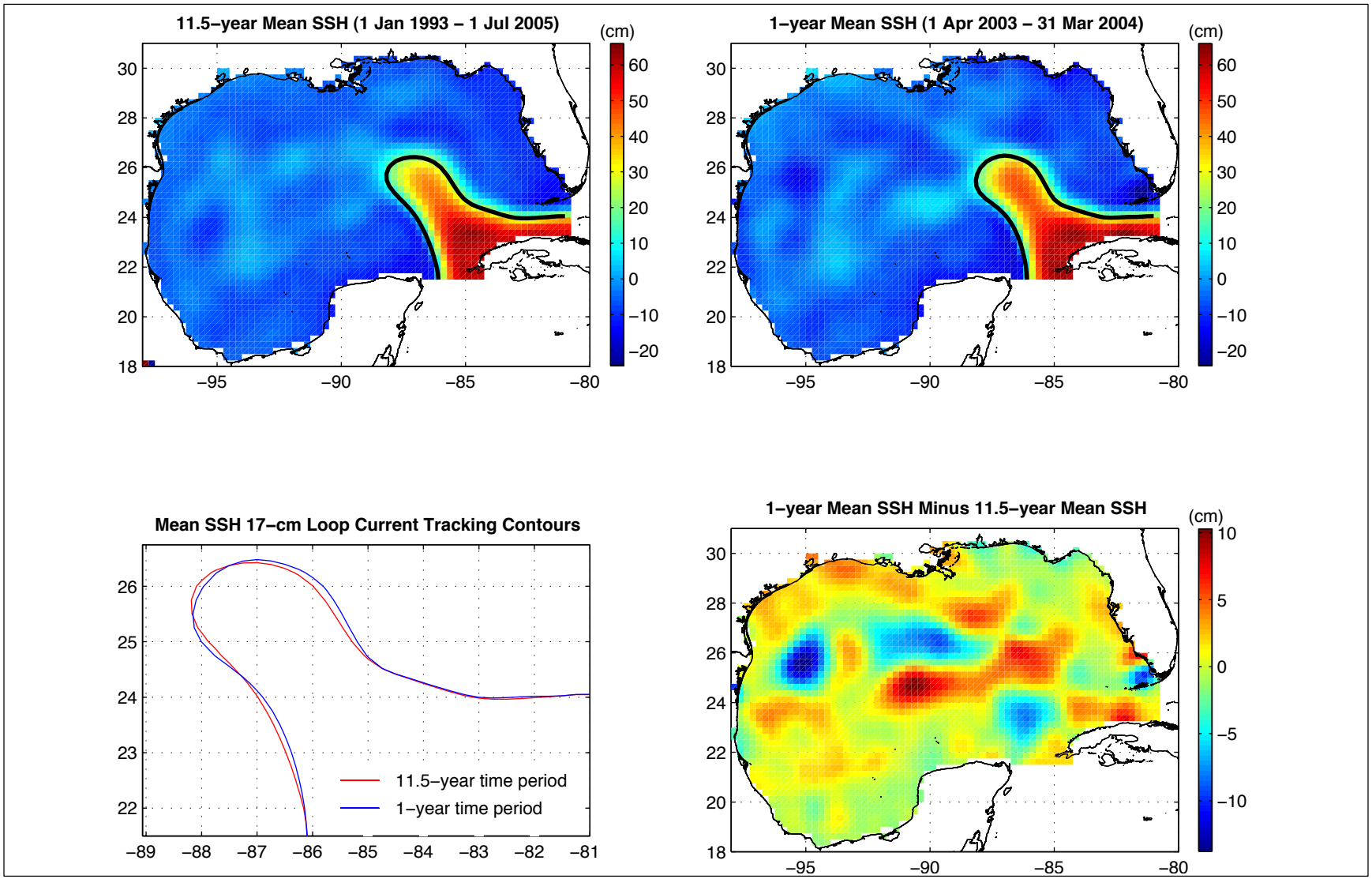

Figure 3-3. Mean SSH fields from the 11.5-year historical record and the 1-year Exploratory Study record are shown in the upper two panels. The mean LC position as determined from the 17-cm LC tracking contour is shown in the lower left panel. The difference of the two mean SSH fields is shown on the lower right panel.

Table 3-1

Ring separation events from the altimetric record: 1 Jan 1993 through 31 March 2004.

Eddy Number	Separation Date	Separation Period (months)	Industry Eddy Name	Area (km^2)	Eddy Maximum SSH (cm)
1	11 Jul 1993	11.5	Whopper	24,183	33
2	10 Sep 1993	2.0	Xtra	38,481	39
3	27 Aug 1994	11.5	Yucatan	43,022	39
4	18 Apr 1995	7.5	Zapp	21,337	36
5	8 Sep 1995	4.5	Aggie	24,899	36
6	14 Mar 1996	6	Biloxi	24,912	32
7	13 Oct 1996	7	Creole	49,644	69
8	30 Sep 1997	11.5	El Dorado	49,229	56
9	22 Mar 1998	5.5	Fourchon	89,143	72
10	2 Oct 1999	18.5	Juggernaut	40,325	39
11	10 Apr 2001	18.5	Millennium	45,705	44
12	22 Sep 2001	5.5	Odessa/Nansen	?	12
13	28 Feb 2002	5.5	Pelagic	22,119	41
14	13 Mar 2002	0.5	Quick	49,936	41
15	5 Aug 2003	17	Sargassum	25,302	49
16	31 Dec 2003	5	Titanic	33,278	43

3.2 Lower Layer

3.2.1 Float Trajectories at Several Levels

Trajectories of all PALFOS floats are shown in Figure 3-4. For the PALFOS floats, CTD profiles were obtained during float surfacing cycles. The PALFOS floats at 1000 m rest depth tend to stay in the central basin for a relatively long time, although these finally "wander away" as well.

An overall "spaghetti diagram" of all RAFOS floats is shown in Figures 3-5. The RAFOS floats were variously deployed at depths of 1000, 1500, 2000, 2500 and 3000 m. In several cases, floats deployed near the bottom ran aground, suggesting upslope, cross-isobath flow during those intervals. The largest fraction of floats were deployed at 1500 m and 2000 m depths. Although much of the current meter and PIES analysis is concentrated in the main study area, these drifter tracks allow a broader perspective on larger-scale circulation in the GOM.

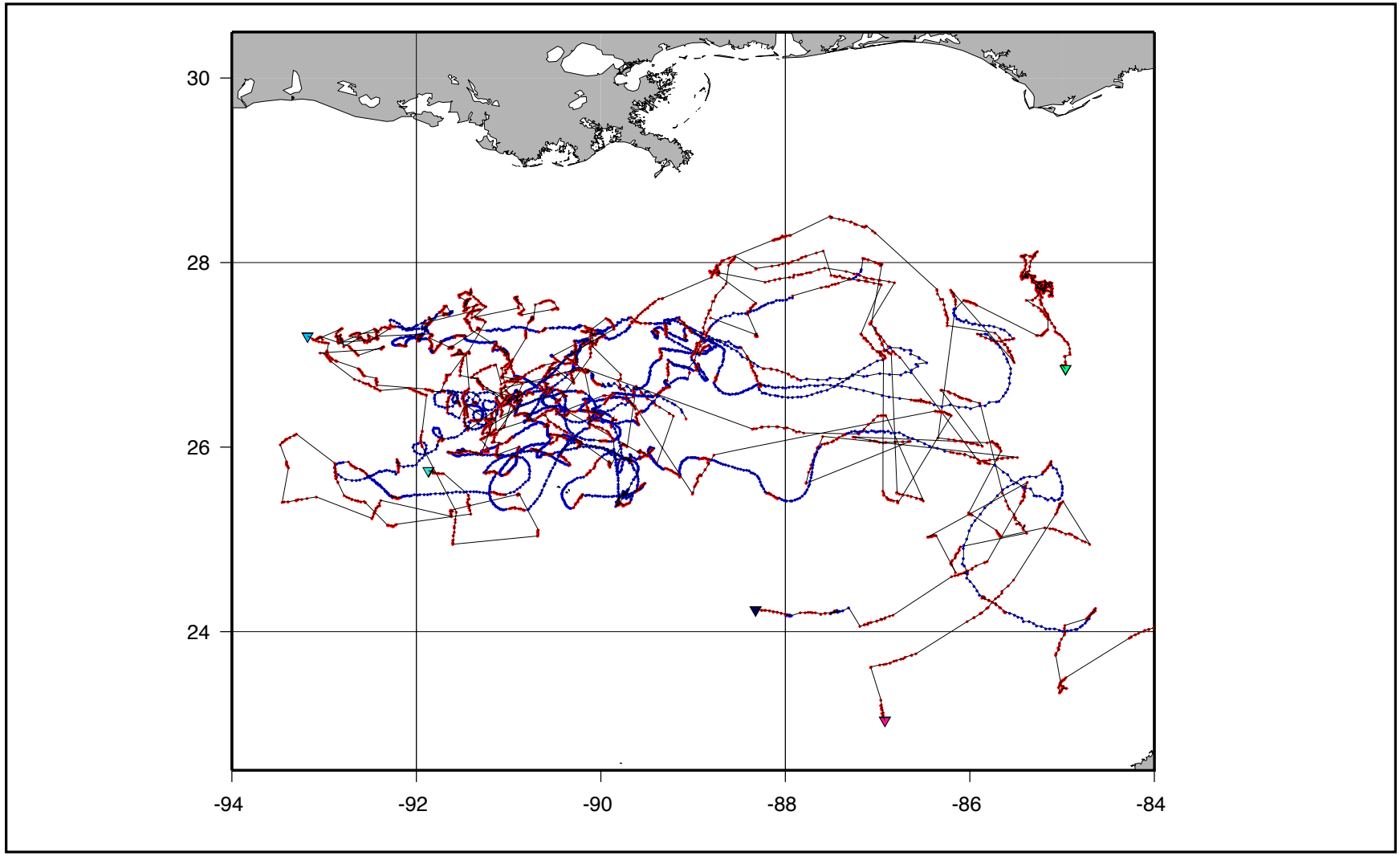

Figure 3-4. Cumulative PALFOS drifter tracks. Time on the surface is sown as red dots, postions at depth as blue dots. When positions at depth could not be determined the sequential locations are jointed by a straight line. The PALFOS drifters had a considerable time in residence in the study area. Note lack of drifters moving into the western basin.

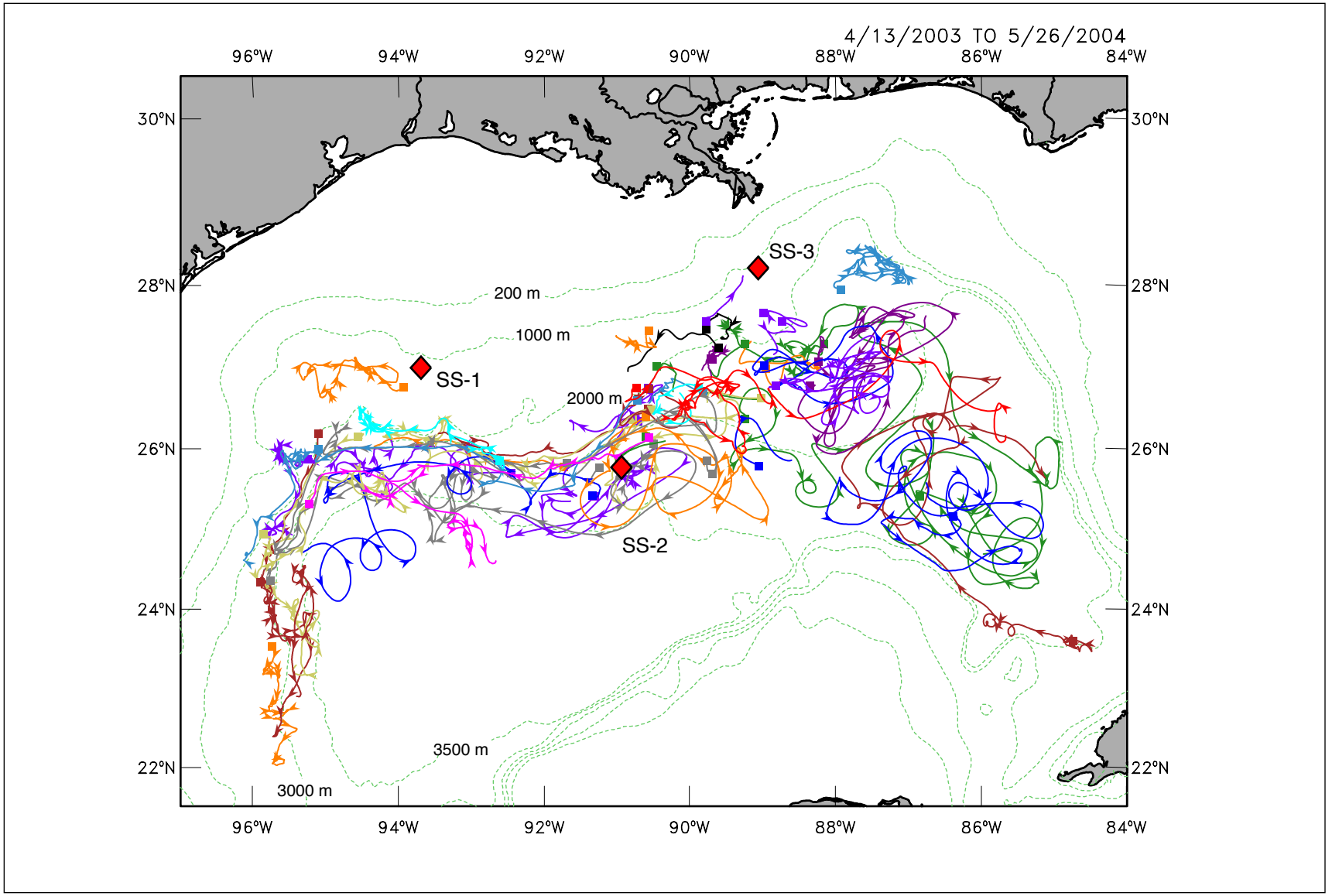

Figure 3-5. Spaghetti plot of all RAFOS float trajectories at all depths in the Exploratory Study. Sound sources in this and other drifter figures are SS-1, SS-2 and SS-3. Track beginning is indicated by a square. Tracks before and after sound source replacement are both shown in this color-coded presentation.

4.0 GENERAL OCEAN CONDITIONS IN THE STUDY AREA

Prior studies (Hamilton et al., 2003) have shown that over the deeper continental slope and rise, the water column is generally partitioned into an upper layer (nominally above approximately 1000 m) and a deeper layer (from approximately 1000 m below the water surface to the local bottom). Material in this report section organizes and presents material based on these vertical zones (upper and lower) since conditions within a zone are generally related while conditions between vertical zones often appear unrelated. The linkage between the vertical zones is a topic of continuing and ongoing study in this and other projects in the GOM.

4.1 Upper Layer Currents and Events in the Study Area

The present study area is directly affected by the LC, LCE and boundary eddies and cyclones. To establish the sequence of conditions during these field measurements, a listing of events has been compiled (Table 4-1) with SSH images corresponding to many of the more significant items in the listing (Figure 4-1). This combination of listing and images provides a convenient visualization to serve as a reference during the subsequent discussions.

4.1.1 Vertical Structure of Upper-Ocean Features

The PIES array enables reconstructing the horizontal and vertical structure of ocean features that provide a general overview of four types of upper-ocean features present in the Exploratory array: LC (Figure 4-2), LCE Sargassum (Figure 4-3) and Titanic (Figure 4-4). Each of these figures show surface velocity field with one or more SSH contour representing the perimeter of an anticyclonic or cyclonic feature. This contour was chosen as the SSH value that most closely coincided with the velocity maxima of each feature. A vertical temperature section is provided with each snapshot as well as the average speed around the perimeter. Also included is the vertical profile of mean speed around the periphery of each feature. The lower depth limit has been chosen as 1500 dbar to highlight the upper ocean structure. Beneath 1500 dbar, deep eddies and topographic Rossby waves dominate the current structure.

The most vigorous feature is the LC: surface speeds near 80 $cm \cdot s^{-1}$, radii near 100 km and Rossby number near 0.1. In contrast to the cyclones, both the LC and the LCE have strong vertical shears that decreased rapidly with depth. Typically speeds decreased by 85 percent from surface to 1500 dbar. Eddy Sargassum has comparable vertical shears to the LC consistent with the fact Eddy Sargassum was sampled so soon after detachment. In contrast, Eddy Titantic was observed to have much weaker speeds and shears compared to Eddy Sargassum. This could be due to Titanic's presence at the edge of our PIES array. Cyclones had little vertical shear. Typically the strongest cyclones were found in the southeast corner of the array adjacent to the LC. Surface speeds range from 20 to 60 $cm \cdot s^{-1}$ and typically decrease by only 70 percent from surface to 1500 dbar. Radii are small being between 35 and 70 km which is close to the present instrumentation's horizontal resolution.

Table 4-1

Timeline of Oceanographic Events During Exploratory Study.

Event	Date	Comments
LC intrusion reaching array	26 Mar 2003	
LCFE Events #1 and #2	30 April to 21 May 2003	LCFE detected by PIES
Detachment and Reattachment of Eddy Sargassum	25 May 2003	Brief surface flow detachment seen in ocean color imagery.
LCFE intensification and Eddy Sargassum/Unnamed Eddy splitting event	19 May – 1 Aug 2003	Cyclone originated on western flank of LC.
Separation of Unnamed Eddy (anticyclone)	25 Jul 2003	Defined by breaking of 17-cm SSH contour
Detachment and Reattachment of Eddy Sargassum	13 Jul – 19 Jul 2003	Observed in MODIS color imagery
Separation of Eddy Sargassum	29 Aug 2003	Observed in MODIS color imagery
Eddy Sargassum center within study array	5 Aug – 1 Nov 2003	Center tracked with PIES SSH
Eddy Sargassum exits study array	20 Nov 2003	Eddy surface signature tracked in satellite imagery.
Detachment and Reattachment of Eddy Titanic	25 Sep - 28 Nov 2003	Defined 17-cm SSH contour, in good agreement with imagery.
Merging of Eddy Unnamed and Eddy Sargassum	17 Oct – 17 Nov 2003	Merging identified in SST and color imagery and change in SSH signatures.
Separation of Eddy Titanic	31 Dec 2003	Defined by breaking of 17-cm SSH contour with no subsequent reattachment
Eddy Titanic northern flank propagates eastward within SE corner of PIES array	2 Jan 2004 – 30 Jan 2004	Eddy Titanic was an elliptical eddy at this time and rotating clockwise.
Cyclone-dominated flow within study array	1 Feb 2004 – 29 Feb 2004	-15 cm amplitude cyclone observed by PIES in center of array
Eddy Titanic northern flank in SW corner of array	1 Mar 2004 – Mar 30 2004	Elongation and rotation once again brought northern edge of eddy into array.

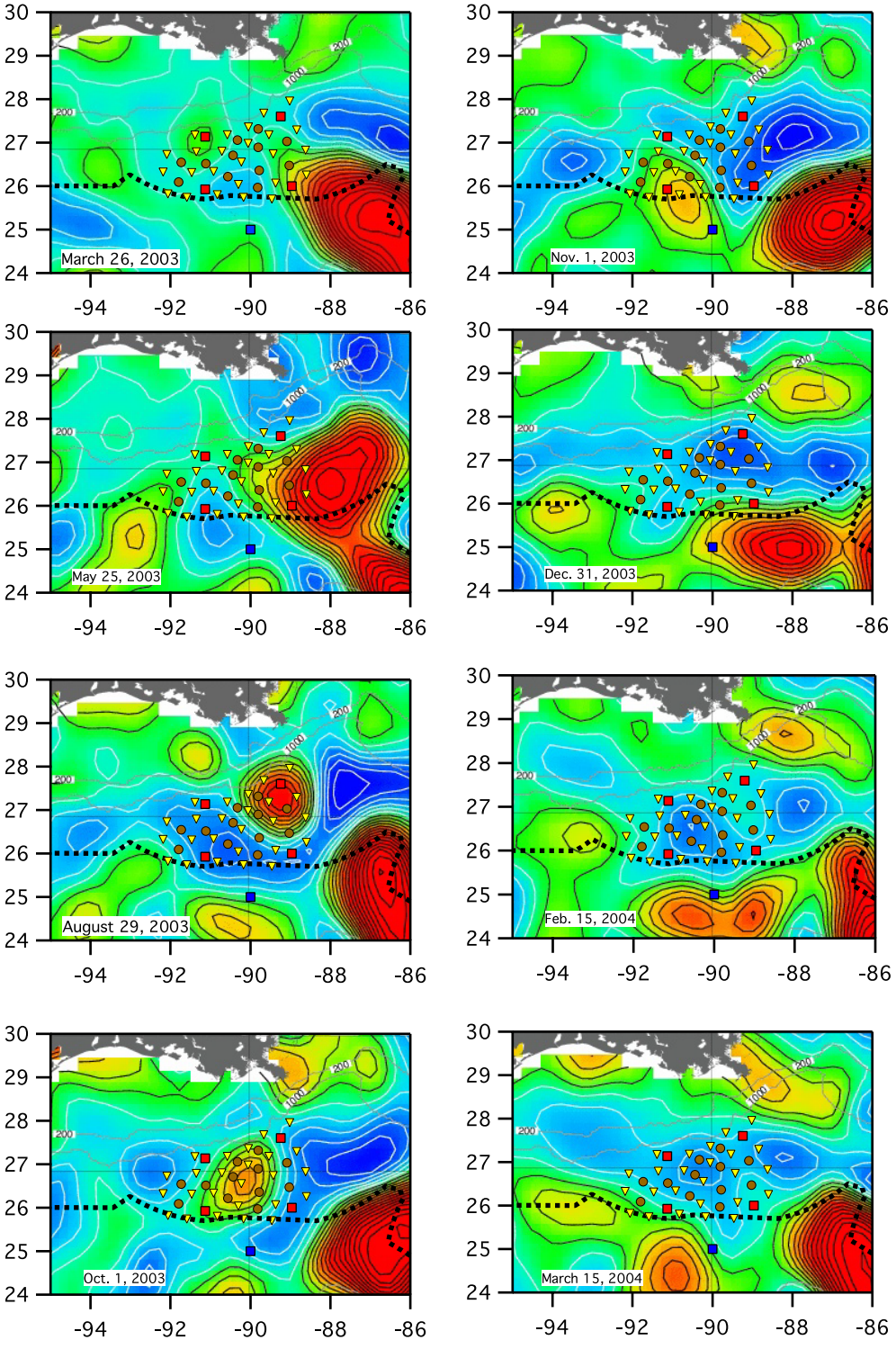

Figure 4-1. Images showing contoured SSH for indicated dates and intervals identified in Table 4-1. In this image, warm colors (red/yellow) are for higher SSHs and cool colors (green/blue) are for lower SSH. The dashed black line is the EEZ. Filled squares are full depth moorings, filled circles are near-bottom moorings and inverted triangles are PIES.

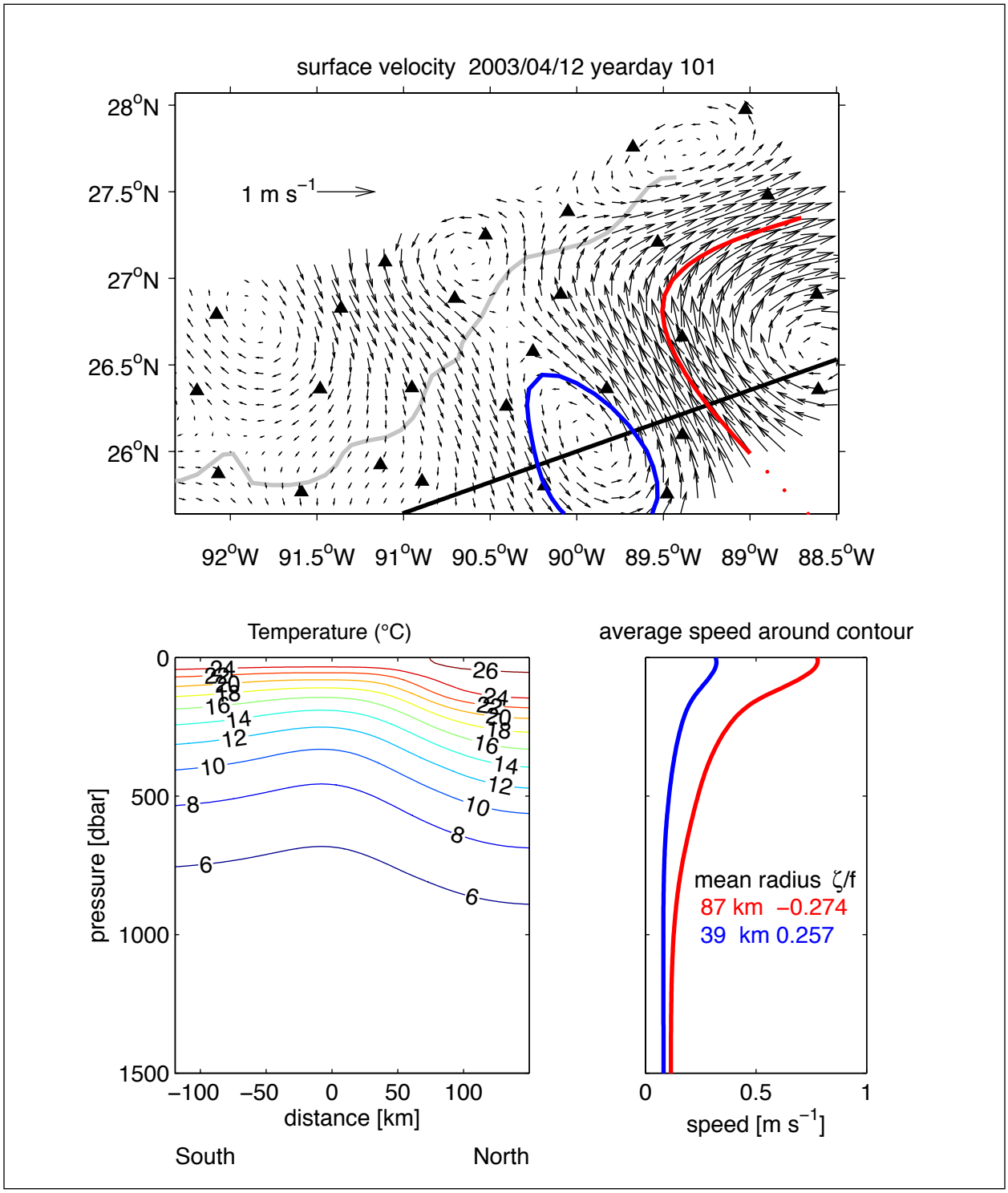

Figure 4-2. Top panel: Surface velocity vectors for 12 April 2003. PIES locations shown with triangles. Sigsbee Escarpment indicated with thick gray line. SSH contours are those that most closely coincided with the maximum surface speeds of LC (red) and adjacent cyclone (blue). Bottom left: Temperature contoured as a function of pressure and distance along the black line in the top panel. Bottom right: Average speed around the SSH contours shown in the top panel.

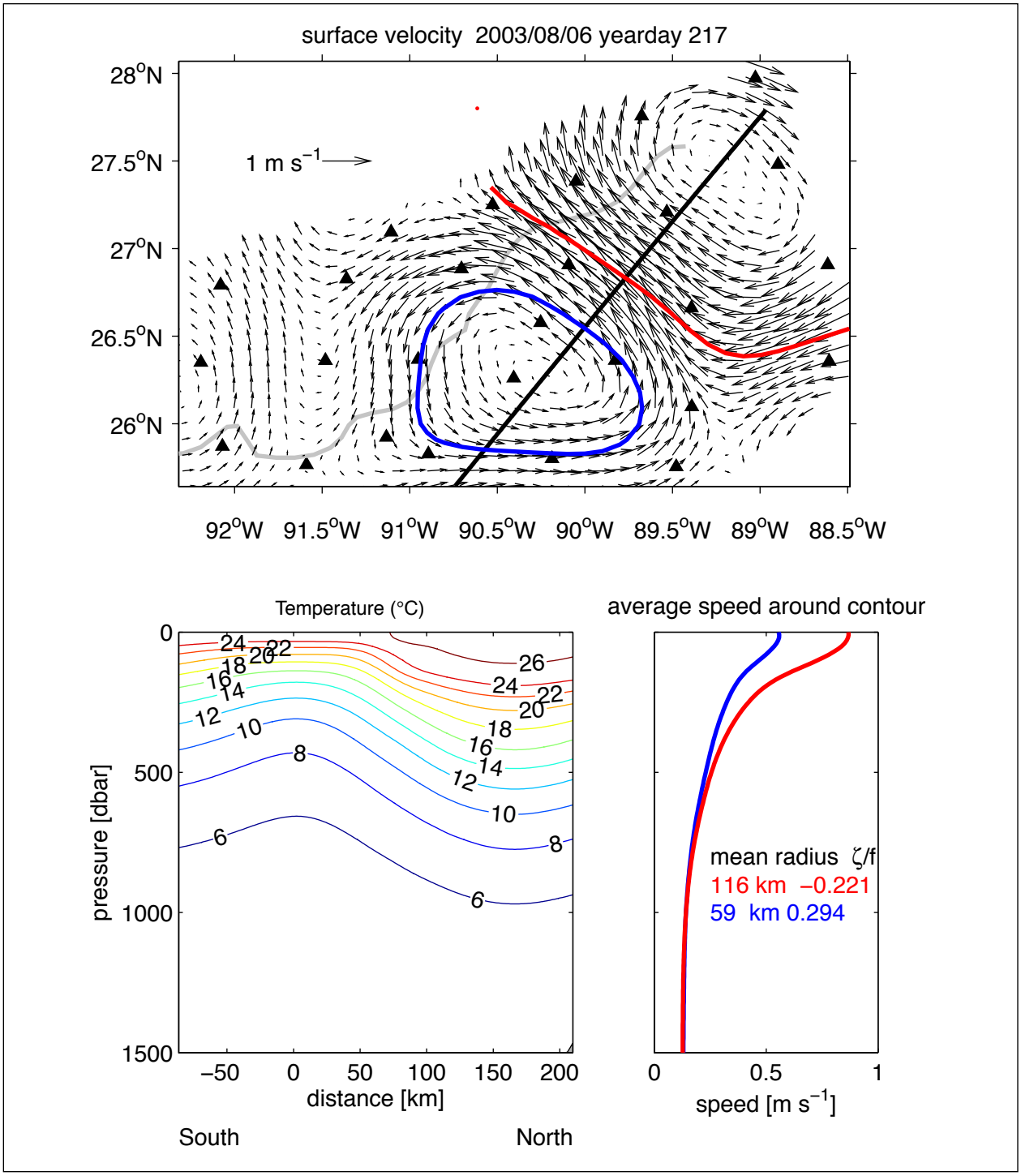

Figure 4-3. Top panel: Surface velocity vectors for 8 August 2003. PIES locations shown with triangles. Sigsbee Escarpment indicated with a gray line. SSH contours are those that most closely coincide with the maximum surface speeds of Eddy Sargassum (red) and adjacent cyclone (blue). Bottom left panel: Temperature contoured as a function of pressure and distance along the thick black line in the top panel. Bottom right panel: Average speed around the SSH contours shown in the top panel.

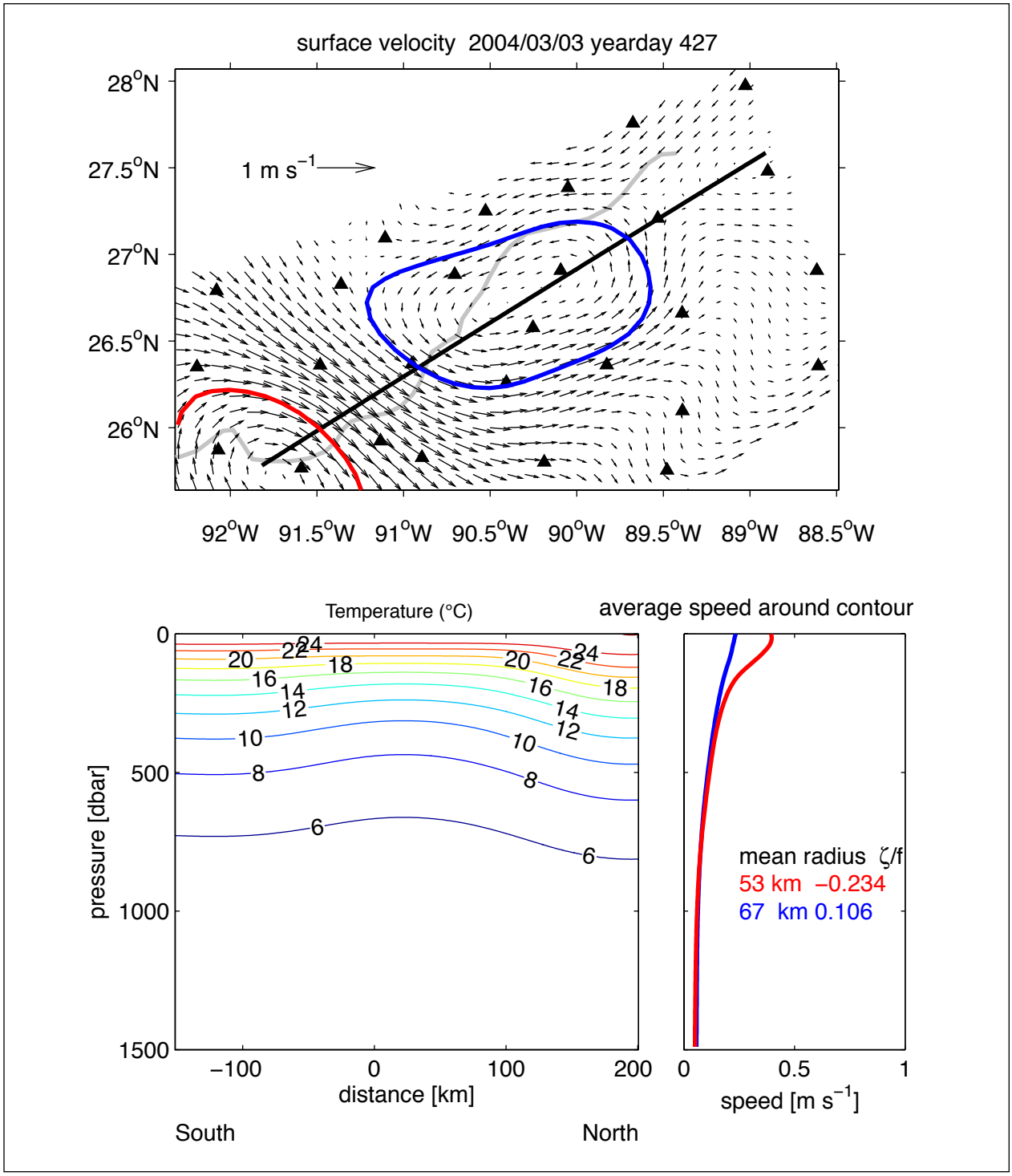

Figure 4-4. Top panel: Surface velocity vectors for 3 March 2003. PIES locations shown with triangles. Sigsbee Escarpment indicated with a gray line. SSH contours are those that most closely coincide with the maximum surface speeds of Eddy Titantic (red) and weak cyclonic flow (blue). Bottom left panel: Temperature contoured as a function of pressure and distance along the black line in the top panel. Bottom right panel: Average speed around the contours shown in the top panel.

4.1.2 Upper Layer Statistics

Statistics for the upper-layer currents and their variability observed in the Exploratory Study array are illustrated by the moored current observations at several levels in the upper water column, and summarized for three levels, the sea surface (0 m), the base of the seasonal thermocline (150 m), and within the main thermocline (500 m). For comparison, the PIES data can map absolute currents daily on these depths and on any other desired depths at a grid of locations within the study area.

4.1.2.1 Upper-Layer Statistics from Moored Current Meters

The presence of the LC and LCE core water is generally shown by: high temperatures greater than 25, 20 and 17°C for the 75, 150 and 225 m instruments, respectively; strong currents in the upper 400 m that decreased with increasing depth; and salinities at 150 and 225 m that were greater than 36.5 and also exceeded the salinities at 75 m. The later is the signature of subtropical underwater (SUW) that enters the Gulf around 100 to 200 m depth with the LC through the Yucatan Channel. LC eddies often have a slightly fresher surface layer and this is reflected by the decrease in salinity at the 75-m level by about 0.2 PSU when an eddy is present. These features of eddy circulations are clearly seen in the L1 records, during June through September 2003, for Eddy Sargassum. At L1, the first half of the record was dominated by the passage of Eddy Sargassum and its associated cyclones.

Some of the above described T/S features were also documented by the profiles taken by the PALFOS drifters. As shown in Figure 4-5, profiles in the LC and in LCEs consistently had the SUW salinity maximum. Also shown is the salinity minimum associated with Antarctic Intermediate Water (AAIW) having a temperature of approximately 6.5° C. The depth of the AAIW varied depending on the upper layer dynamics, e.g. presence of a LCE, or a cyclone, but consistently was in the upper layer since the PALFOS residence depth was 1000 m.

The moorings in deeper water, below the Escarpment (e.g. L3; Figures 4-5,) show the deep lower-layer bottom intensified fluctuations penetrating up to the 750-m level most of the time. All three moorings below the Sigsbee Escarpment had a small number of events of 1 to 2 weeks in duration that appear to be visually coherent through most of the water column. At L3 (Figure 4-5), the beginning of the record ~ August 10 and ~ October 15 had similar northwest and southeast flows, respectively, at all depth levels with some indication of surface intensification. It is difficult to determine if these apparent whole water column events were significant connections or just coincidences between separate upper- and lower-layer flow regimes.

4.1.2.2 PIES-Based Current Statistics

PIES data were used to develop time-averaged mapped currents and streamfunction for this 1-year observational period at three representative upper layer depths. (e.g. in Figures 4-6) The absolute currents for each of these representative levels were generated as the sum of the baroclinic profiles plus the deep reference currents. Those methods produced time series and mean currents that agreed well with all directly-measured currents, at levels within the upper

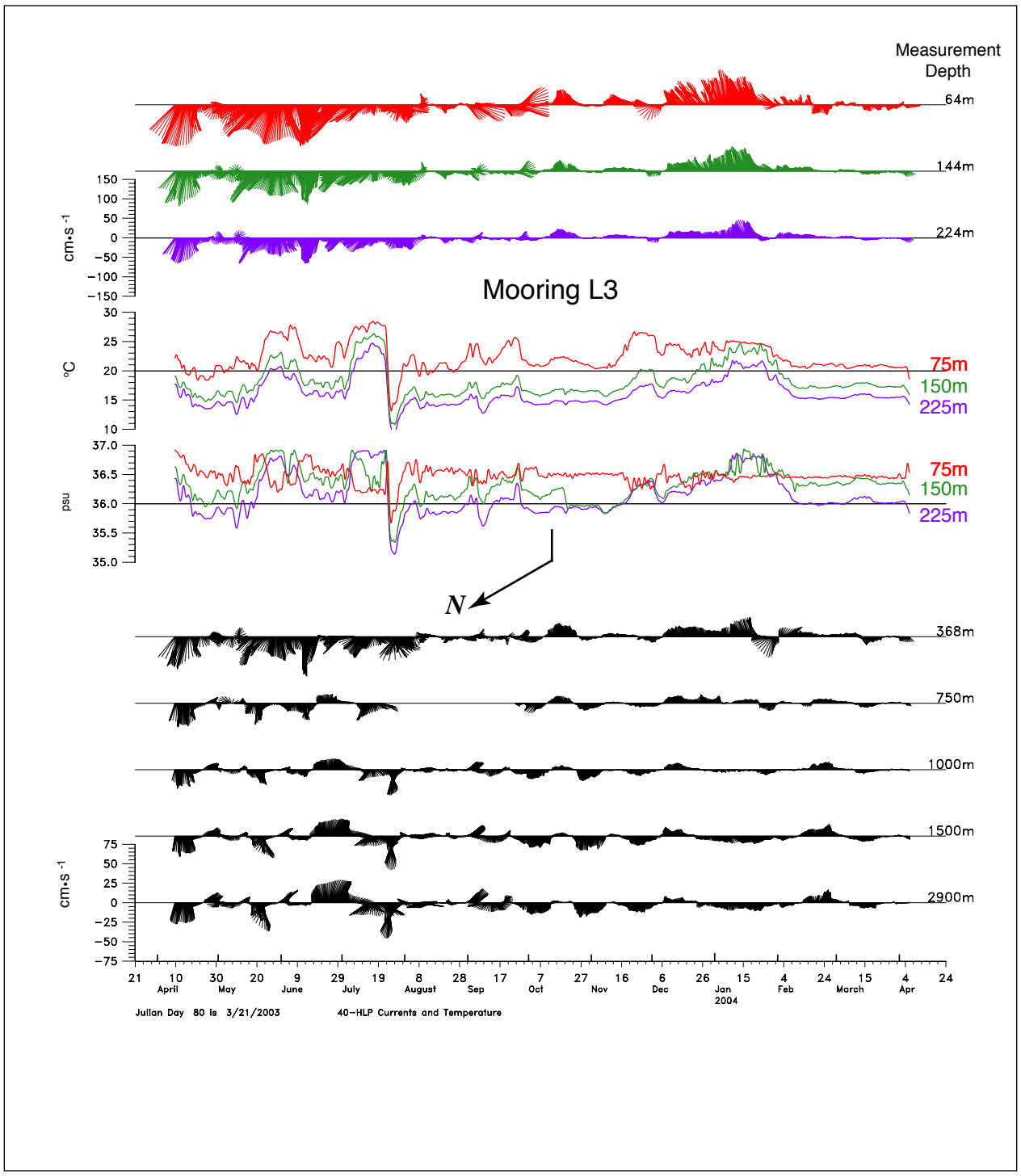

Figure 4-5. 40-HLP current vectors, temperature and salinities for the indicated depths at Mooring L3.

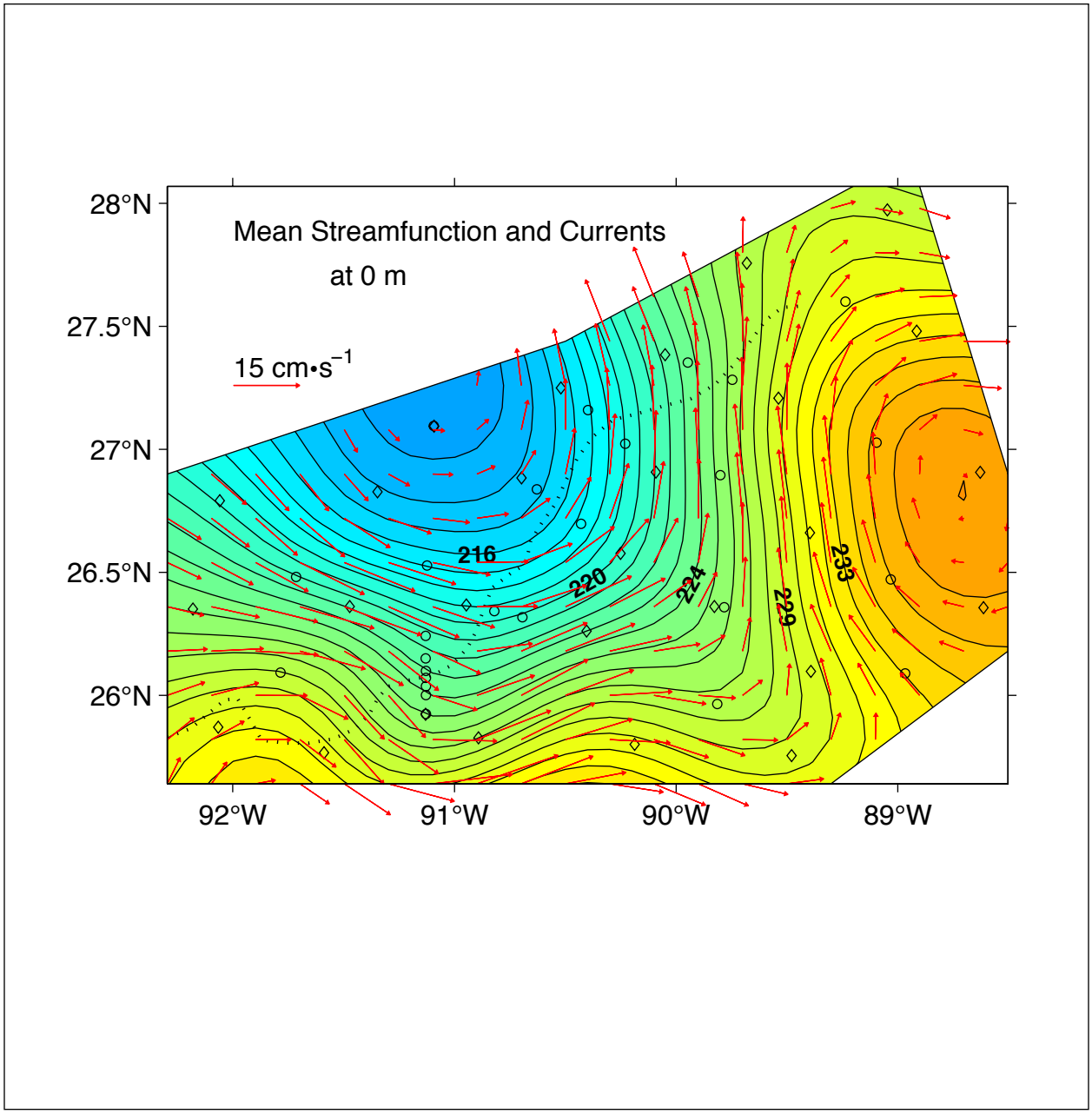

Figure 4-6. Time-average mean streamfunction (contours) and currents (red vectors) at 0-m depth. Dotted line denotes the center of the Sigsbee Escarpment. Streamfunction contoured every 1 km m•s^{-1} with low (high) values shown with blue (red) hues. Currents vectors plotted at 20-km spacing. PIES sites indicated by diamonds; current meter moorings by circles.

layer on five tall moorings, and in the deep layer at these same sites plus 15 deep moorings for a total of twenty sites of deep current observations.

It is important to recognize that the time-average currents were dominated by a few strong events for this year of observations. The maps for one year should not be interpreted to represent the long-term mean currents. The point is that even the 1-year mean currents were event dominated, i.e., the average of only a few big events – accounting for the mean eastward currents all along the southern half of the array west of 90°W.

Values of mean kinetic energy for three representative upper levels, 0 m, 150 m, and 500 m, show the highest values occurred along the edge of the LC where it swept into and out of the study array near 26°N to 27.5°N and 89°W to 90°W. At all three upper levels shown, the mean kinetic energy was much higher south than north of Sigsbee Escarpment. For the two uppermost levels this was because the variability associated with the LC and LCEs was confined to the region south of the Escarpment, and for the 500-m level, on which deep eddy variability contributes significantly, the Sigsbee Escarpment further constrained most deep current variability to its south.

4.2 Description of Deep Layer Currents and Events

4.2.1 Deep Eddy Maps

The most energetic and persistent currents below 1000 m in the study area were associated with cyclonic and anticyclonic eddies that entered the study area from the east and southeast, on trajectories suggestive of an origin near the LC. Typically, deep eddies were generated near the eastern border under the LC and associated with its events of strong variability.

During times when the LC and its peripheral eddies and meanders were southeast of the study array, the deep eddies appear to have originated there also, because they entered the study array near its southeast edges and followed trajectories to the northwest. When the LC protruded unusually far north, during July – September 2003, its strong peripheral eddies and meanders occurred due east of the study array. Coincidentally deep eddies, both cyclonic and anticyclonic, were then generated and entered the study array along its eastern border.

Once west of 89°W, deep eddies typically translated northwest until they encountered the Sigsbee Escarpment, whereupon their behavior differed depending upon whether the deep eddy was cyclonic or anticyclonic. Figure 4-7 [15 December to 25 December 2003] illustrates one of several cases in which a strong deep cyclone approached the Sigsbee Escarpment, whereupon its path deflected to the left (west). Figure 4-8 illustrates the current and temperature structure associated with this deep cyclonic eddy. The upper left and right panels show respectively the surface and deep velocities and streamfunction for 23 December 2003. It illustrates how different the patterns of horizontal currents can be in the upper and deep layers on a given day. This moderately strong deep eddy with currents up to 35 $cm \cdot s^{-1}$ had little expression at the surface. This point is further emphasized in the bottom panel by the temperature section along 90°W which crossed the eddy. The deep currents had little vertical shear, and consequently (being geostrophic) little expression in the temperature structure. This contrasts with a strong

deep anticyclone approaching the Sigsbee Escarpment where its path deflected slightly to the right. Deep anticyclones encountering Sigsbee Escarpment typically stalled and decayed rather than propagate away. In addition to deep eddies that propagate into the study array, some cyclonic and anticyclonic features intensified in place.

4.2.2 Deep Currents

Deep, low-frequency current fluctuations, as measured by instruments 100 and 500 m from the bottom on the short moorings and at various depths below 1000 m on the tall moorings, were extraordinarily inhomogeneous. The Escarpment divides the array approximately in half and currents above and below differ in character and energy. There were also differences in the character of the fluctuations from the eastern and western sides of the array. These deep fluctuations will be interpreted in terms of propagating topographic Rossby waves (TRW) in subsequent chapters.

Along a transect approximately normal to the Escarpment (from L3 to L2 in Figure 2-1), current amplitudes decreased substantially with the largest decrease occurring at the Escarpment. Currents above the Escarpment had shorter period fluctuations. Currents at the top of the Escarpment (M3) rarely reversed resulting in a mean flow to the southwest. A major event at M3 (July 2003) resulted in current fluctuations that were similar to TRW wave trains as described by Hamilton et al. (2003, 2005). It appears that, in general, the Escarpment insulated the above Escarpment (shallower regions) from the more energetic currents in the deeper water, especially on the lower half and base of the Escarpment. The pattern of currents fluctuations suggest that kinetic energy was being converted to mean flow in the vicinity of the Escarpment, particularly where it was steep in the southwestern part of the mooring array.

The transect along the western side of the array also contrasts conditions below and above the Escarpment. This transect contained the SEBECP moorings on the Sigsbee Escarpment. The currents at 200 m above the bottom at S3 and S5 are given in Figure 4-9. The mooring in the middle of the Escarpment slope (S3) had the strongest currents, and similar to M3, flows almost never reversed so there was a large residual flow along the Escarpment towards the southwest. The signal at S5, on the top of the Escarpment slope, was similar to that at S3, but with decreased amplitudes. The periods of the fluctuations on and below (S5, S3 and L4) the Escarpment were much longer (~ 1-2 months) than either the fluctuations in the southwest corner of the array or above the Escarpment at N5 and L2. The amplitudes of the currents at the latter two moorings were small when compared with the moorings on or below the Escarpment.

To illustrate how closely the high velocity mean jet was associated with the Escarpment, the bottom along-slope currents from the SEBCEP transect (S1 to S6, plus L4 and N5) are plotted and contoured, with some subjective interpolation, in Figure 4-10. Note that the bottom instruments on the S moorings were only 3-m above the bottom and thus well within the bottom frictional boundary layer. The along-slope means over the steepest part of the Escarpment were approximately double those immediately above and below. The highest mean speed observed was 200 m above the bottom at S3. This suggests that the mean jet was centered over the steep part of the slope or possibly near the base (i.e., S2) and decayed rapidly with distance from the Escarpment. It is not known how far up into the water column these enhanced flows may have

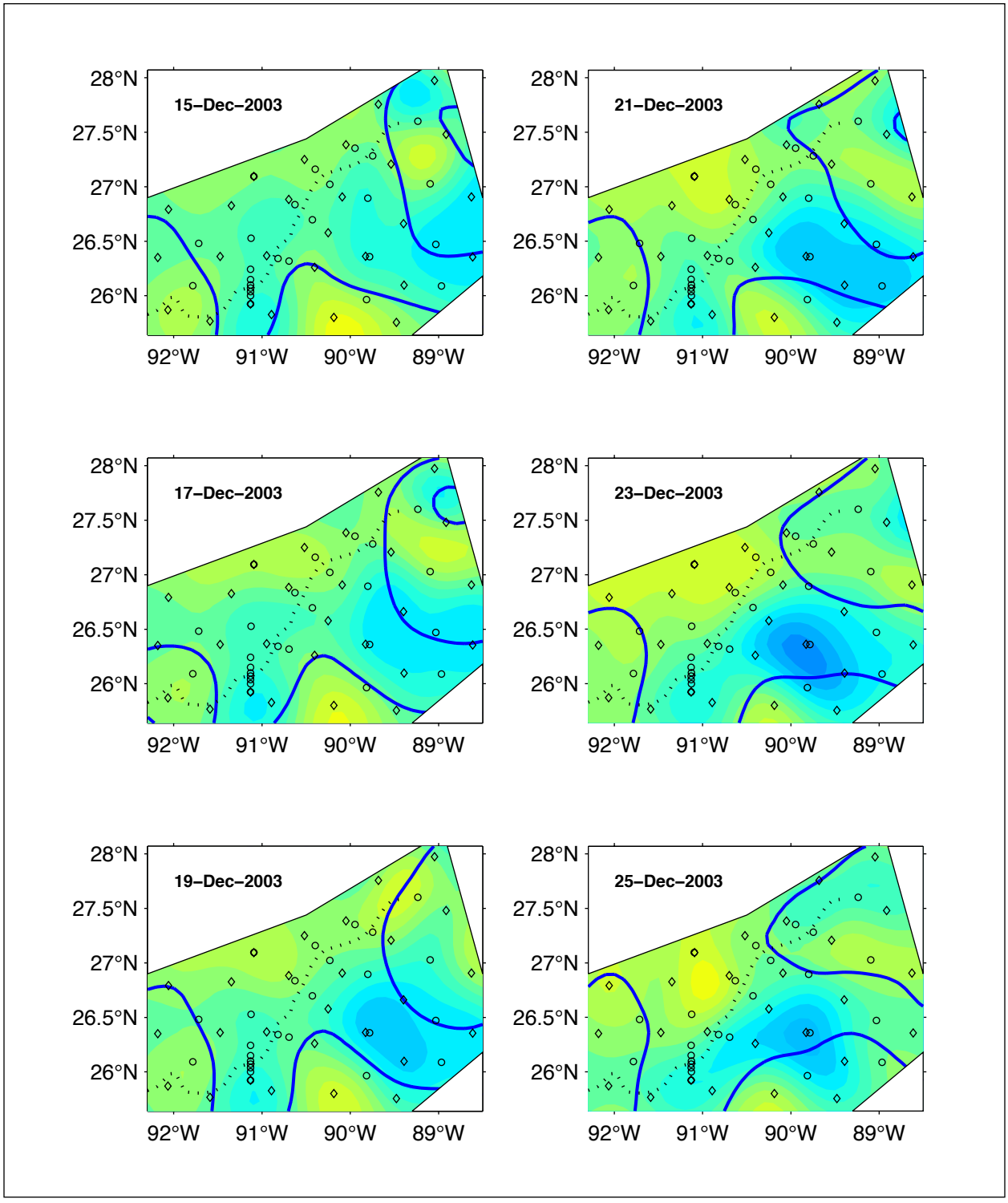

Figure 4-7. Case study: A deep cyclone propagates along the Sigsbee Escarpment [15-25 December 2003]. Maps of surface streamfunction (bold contour lines) superimposed on shaded contours of 1500-m depth pressure for six separate days. The sequence begins with the top left panel. The dotted line denotes the center of the Sigsbee Escarpment. PIES sites indicated by diamonds; current meter moorings by circles.

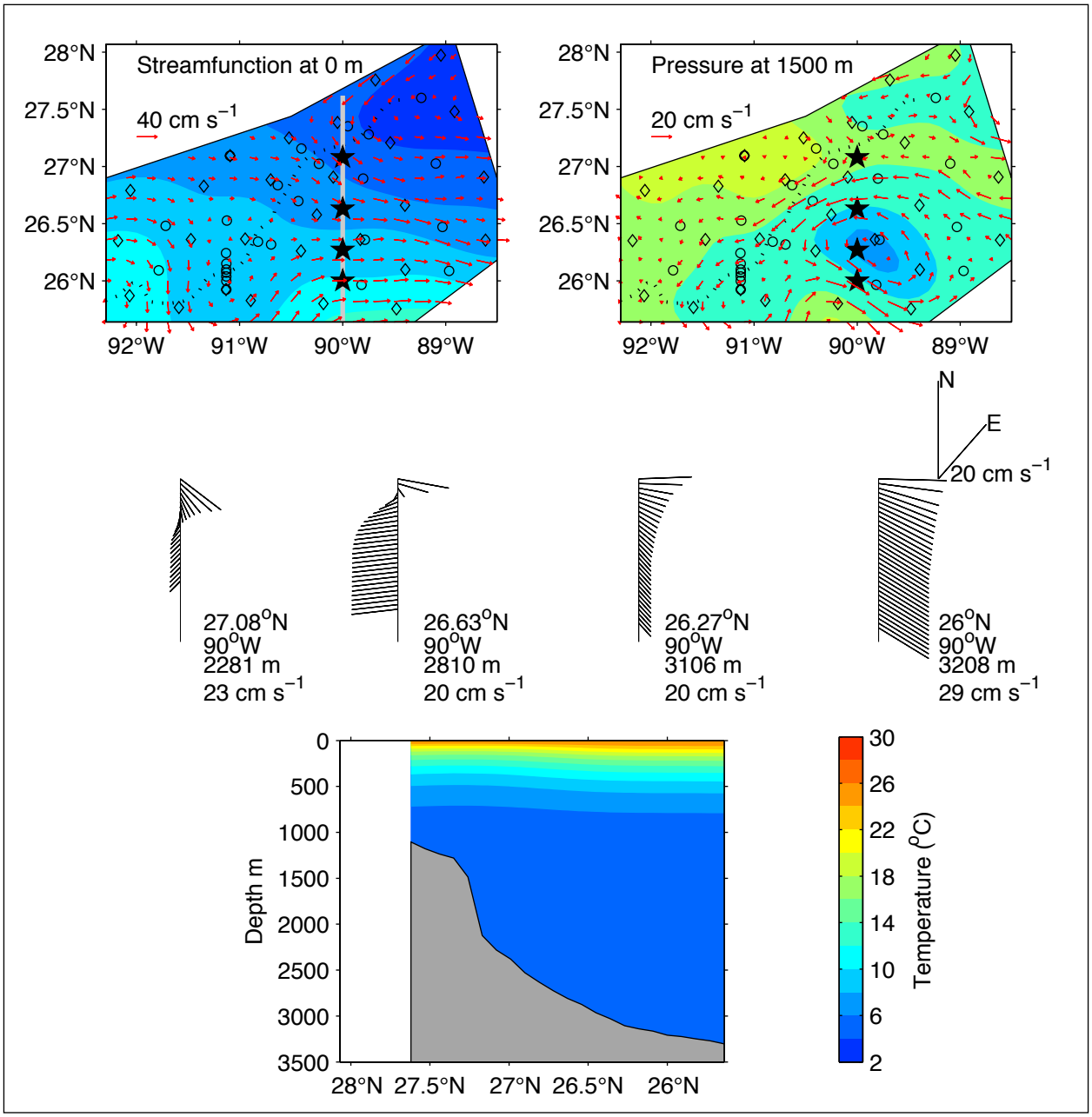

Figure 4-8. Several views of current and temperature structure in the region for December 23, 2003 provided by PIES and deep current measurements. Top panels: Streamfunction at the sea surface (left) and pressure at 1500 m (right) in plan view. Contour intervals are 5 km m•s^{-1} and 0.02 dbar, respectively. Anticyclonic circulations are shown by reddish hues; cyclonic circulations by bluish hues. Currents vectors plotted at 20-km spacing. PIES sites denoted by the diamonds; current meter moorings indicated by the circles. A dotted line marks the center of the Sigsbee Escarpment. Middle panels: Vector profiles of absolute velocity every 100 m from the surface to the bottom at four locations indicated by the solid black stars in top panels. Latitude, longitude, bottom depth, and surface speed at each location are noted. Bottom panel: Cross-section of temperature in °C along the gray line in the top left panel.

occurred. Away from the slope on the deep side of the Escarpment, the means were largely depth independent below 1000 m (Figure 4-9).

4.2.2.1 Float Trajectories in Array

The majority of the RAFOS floats were deployed within the domain of the instrumented array, and in the vicinity of the Sigsbee Escarpment. The average behavior of a float depended on its location within this region. Northwest of the Escarpment, the trajectories indicate that the flow was slow and unsteady, while to the southeast the flow was more energetic and marked by loops and eddies. Floats in the southwest corner of this region showed steady motion to the southwest, parallel to topography. Only a few floats appear to have crossed the steep topographic gradients of the Escarpment. The character of the float trajectories at 2000 and 2500 m was similar to that found in the shallower levels. The Escarpment was an effective barrier for the deeper floats since, out of 19 occasions when floats were at the Escarpment, in only three instances did the float (all at 1500 dbars) cross from one side to the other. The float trajectories generally followed the dynamical topography of the PIES pressure fields.

A general east-west asymmetry was observed in the tracks, with the floats that traveled to the east spreading over most of the eastern basin, while those that went to the west tended to concentrate against steep topography (Figure 3-5). Several westward moving floats in fact followed the bathymetric contours extremely closely and make excursions into and around submarine canyons such as Alaminos Canyon in the vicinity of 26°N, 95°W (float 465 at 1500 meters and float 480 at 1900 m).

4.2.3 Bottom Pressure Common Mode

An array-wide, 16-day, coherent bottom-pressure signal, referred to as the common mode, was removed from the bottom pressures before mapping deep pressure, streamfunction, and velocity in order to enhance and reveal deep mesoscale features. The common mode is the array-wide average of the bottom pressure records. This signal was coherent across the array and therefore had very weak associated pressure gradients and hence essentially no velocity signal.

4.2.4 Mapped Current Statistics at 1500 m and H-100 m

Maps of the time-average currents and streamfunctions derived from PIES-based observations for this 1-year observational period at two lower-layer depths show that currents were relatively uniform in the vertical below 1500 m. A variety of cyclonic and anticyclonic deep eddies entered the study array, mainly confined south of Sigsbee Escarpment; the most prevalent and strongest eddies were cyclonic. We can account for the three time-averaged cyclonic regions in the one-year mean. The mean feature near 26°N 89.5°W arose because strong cyclones entered repeatedly near this location from the southeast. The mean feature near 25.8°N 91°W arose because several cyclones lingered near this location during their general southwestward transits during the year. The time-averaged cyclonic feature along the eastern edge arose because numerous weak cyclonic eddies and few anticyclonic features appeared there. The strongest mean deep currents were about 10 $cm \cdot s^{-1}$ southwestward along the base of Sigsbee Escarpment near 26°N 91.5°W which is consistent with the local stronger currents described in Section 4.2.2.

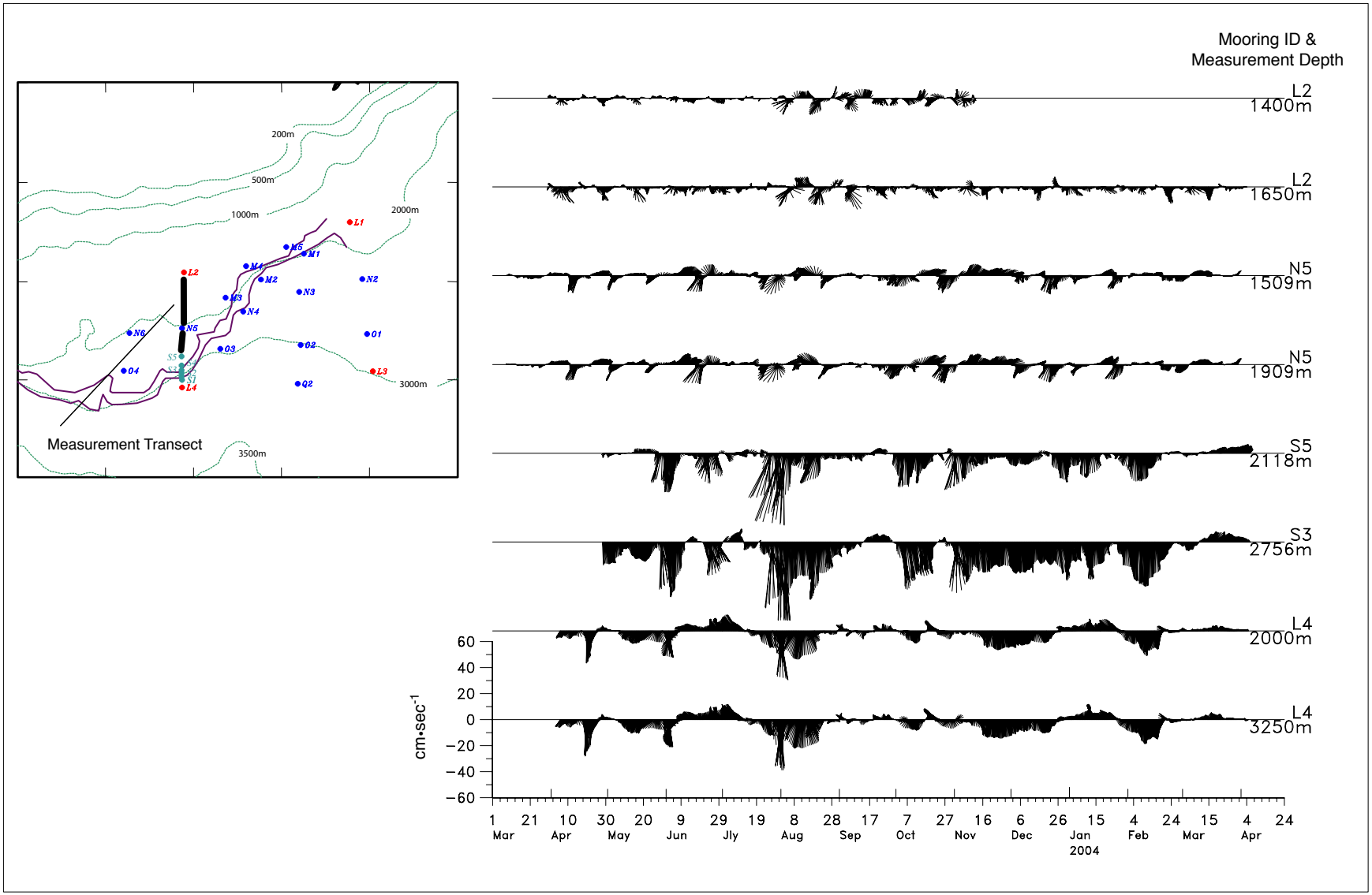

Figure 4-9. Near-bottom 40-HLP current vectors from nominally 100 and 500 m above the seabed for the indicated moorings along the transect from L4 to L2 (see inset map). Up is directed along the general trend of the isobaths at each location (i.e. approximately eastward or northeastward).

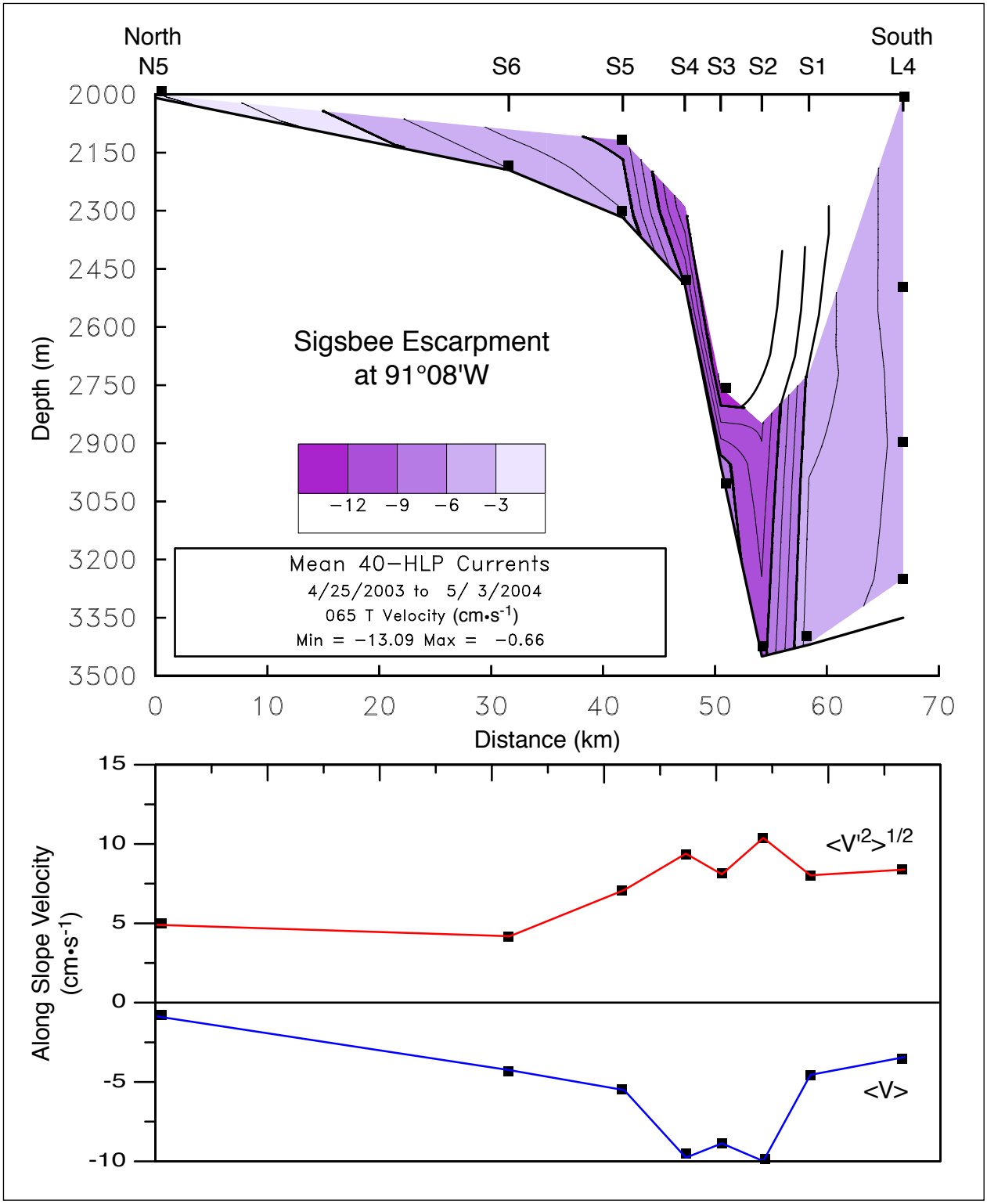

Figure 4-10. Upper panel: Contoured mean along-slope 40-HLP current velocity component (065°T) from the Exploratory and SEBCEP studies. Measurement positions are indicated by the solid squares. Lower panel: Along slope mean velocity (blue line) and standard deviation (red line) from the bottom-most instrument on each mooring. Negative velocities are towards the southwest.

North of the Sigsbee Escarpment the time-averaged currents tended to be southwestward at 3 – 5 $cm \cdot s^{-1}$. These means arose as the sum of the passage of several strong cyclones with their low pressure centers remaining south of Sigsbee Escarpment, and with their northwestern sector having peripheral currents to the southwest.

4.3 Extreme Events in the Deep Currents

For engineering purposes, it is useful to give the observed maximum speeds as an indication of the strength of extreme currents that might be encountered in the lower layer. Maximum speeds were calculated for the complete current-meter array using the 3-HLP records at 100 m from the bottom, except the 500-m and 200-m levels (S3 and S5 only) were substituted if the lower records were incomplete for the year. The results are given in Figure 4-11. The pattern of extreme velocity magnitudes is similar to that for the 40-HLP kinetic energy with maximums occurring just below or on the Escarpment in two separate regions, one in the northeast and the other in the southwest. The former region has a tongue stretching along the Escarpment towards the west-southwest. Maximum speeds were observed at M1 (67 $cm \cdot s^{-1}$) and S3 (66 $cm \cdot s^{-1}$). The lowest maximum speeds were west (above) of the Escarpment at N6 (16 $cm \cdot s^{-1}$). The percent time that the currents were in the upper quartile of their speed range were also calculated for each mooring. The results range for about 0.5 to 1.5% of the records, which correspond to between 40 and 120 hours, not necessarily consecutive, out of a year that the currents exceed 75% of the observed maximum speed.

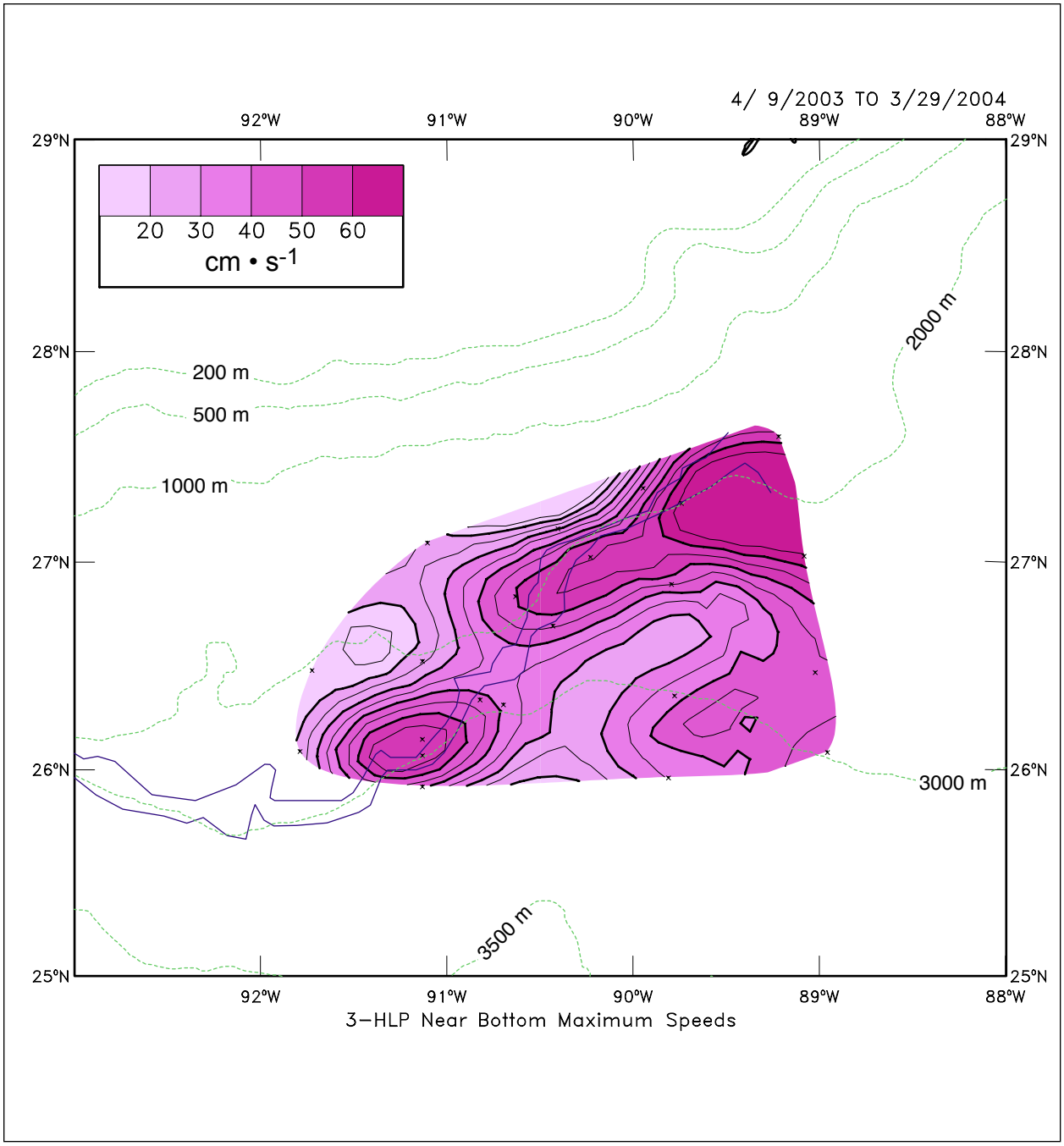

Figure 4-11. Maximum current speeds at instruments 100 to 500 m above the bottom. Calculations used 3-HLP records.

5.0 INTERPRETATION AND ANALYSIS

5.1 Upper Layer

5.1.1 Upper Ocean Eddy Kinematics and Dynamics

Dynamical interpretation of the upper ocean circulation can be difficult given the complexity the eddy interactions in and around the study region during the Exploratory Study – an eddy field that can be best characterized as an energetic nonlinear flow, at least during the first half of the program time period. The description of the upper-layer circulation might be quite different if the LC had exhibited a canonical LC eddy shedding cycle during the study time period while remaining primarily south of the study region. A canonical LC eddy shedding cycle, consisting of a modest northern intrusion, eddy separation and retreat, would probably have exhibited a more quiescent surface eddy field in the study array much like what was observed later in the field program. Instead, as we have noted in the historical perspective presented in Chapter III, one of the most northerly and energetic intrusions was observed. This event significantly impacted the upper ocean circulation in the study region.

In Section 4 the upper ocean events were presented from a descriptive physical oceanography viewpoint using the available imagery, PIES altimetry, measured currents and drifters. The observed LC intrusion was remarkably complex, consisting of a deep northern LC intrusion, LCE detachment, LCE reattachment, another LCE detachment, LCE splitting, another brief LCE reattachment, LCE separation and a modest retreat of the LC. This scenario is far more complex than the canonical model. Quantitative estimates for event intensity, areal extent and propagation paths were included in the overview in Section 4, as well as some qualitative kinematic interpretation of the eddy-eddy and eddy-LC interactions, both cyclonic and anticyclonic.

Controlling dynamics of the observed upper ocean flow field was dominated by an energetic LC/LCE intrusion and eddy shedding cycle that is interpreted as a shielded vortex instability (Flierl, 1988). This does not explain all types of instabilities that may occur in the vicinity of the LC, however it does provide a framework within which upper layer motions of LC/LCE vortex system can be evaluated.

5.1.2 Instabilities, Upper Ocean Cyclones and Eddies/Waves

The far northern intrusion of the LC changed the overall evolution and character of the instability. In the observed event, the topographic interactions along the northern margin act as perturbations to the instability and after that point the higher-order azimuthal modes are able to propagate freely clockwise around the periphery of the intruded LC front and around the southern periphery of the closed circulation of the embedded LCE. In the present case, the cyclonic feature is stripped from the LC/LCE system and evolves independently over the continental slope of the north central Gulf.

This instability led to repeated deepening events of the LC deep layer and a commensurate increase in the SSH of the LC/LCE. The times associated with the maximum deepening events were separated by 52 days, which is the same as the interval between the dates of the two

detachments of Eddy Sargassum. Based on this an other evidence the time scales in this evolving instability event range from periods of 50 to 80 days; and, possibly 12 to 27 days, if we divide by 3 or 4 to account for the peripheral disturbance caused by cyclones associated with the dominant instability modes. These periods are commensurate with the frequency bands of the observed TRWs and potentially provide a surface-layer forcing mechanism for the waves. The location of the deepening under the LC/LCE also agrees reasonably well with the backward ray path of the 61-day period TRW.

Of particular interest in the present case is that the lower-layer signal was not able to propagate past the Sigsbee Escarpment as the upper-layer cyclone moved onto the slope. Thus, the cyclone returned to a more upper-layer configuration before it propagated westward toward the western GOM. Of additional relevance to the present case is the fate of the baroclinic cyclone after it left the study area. The main point of this consideration relative to these cyclonic features is the close correspondence between the frequency of the observed baroclinic waves and the 60-day TRWs identified in the study array that suggest a common forcing mechanism which is well explained by the shielded vortex instability mechanism.

5.1.3 PIES SSH Time and Space

In agreement with EOF analysis, most of the barotropic half-power periods were in the range from 14 to 16 days showing clearly that the common mode signal dominated the barotropic signals over the majority of the study region. In the south-central part of the array below the Escarpment the half-power periods ranged from 20 to 35 days, commensurate with one of the energetic TRW frequency bands.

Time scales of the baroclinic and combined barotropic and baroclinic SSH anomaly signals were similar because of the small contribution by the barotropic mode to the total signal. The long half-power periods associated these signals show the dominance of the low-frequency LC and LCE variability in the region during the study. These longer periods, 200 days and greater, were confined to the eastern part of the array and along and near the Escarpment. Regions with the shortest half-power periods, less than 100 days, were found to the northwest of the Escarpment and in southeast part of the array below the Escarpment. This signal likely arose from the higher frequency variability associated with eddies over the continental slope and frontal eddies along the western margin of the intruded LC.

The spatial scales of the barotropic, baroclinic and the total SSH variability in the study region were examined by estimating the first zero-crossing of the spatial correlation function, L_0, from correlations of the PIES time series between stations as a function of distance between the stations (Table 5-1).

Table 5.1

PIES SSH anomaly dominant spatial scales of motion.

	Barotropic Signal	**Baroclinic Signal**	**Total SSH Signal**
	L_0 (km)	L_0 (km)	L_0 (km)
all stations	95	205	215
above Escarpment	120	140	165
below Escarpment	95	195	200

5.1.4 EOF Analysis of Vertical Current Structure and Dynamic Height

Upper-layer currents were dominated by slowly evolving eddy events.. Using time domain EOF analysis at each tall mooring showed that the first mode accounted for between 83 and 94% of the total variance, and the vertical structures of the u and v components are similar at each site. The modes were surface intensified, decaying with depth to small amplitudes (< 10 $cm \cdot s^{-1}$) at 1000 m. The most rapid decay took place in the upper 200 to 300 m.

A time domain EOF analysis was performed using the baroclinic SSH anomaly derived from the PIES array. The purpose was to determine the primary spatial and time scales of the upper-layer eddy circulations that were resolved by the array. The first two modes are significant and accounted for 72 percent of the total variance of baroclinic SSH signal measured by the PIES. The patterns were well resolved by the array spacing. The barotropic part of the SSH anomaly contains signals that relate to depth-independent current fields over the full depth of the water column. The amplitudes of the barotropic SSH fluctuations were about 10 percent of the baroclinic signals.

5.2 Lower Layer

5.2.1 Time Scales of Deep Currents

Previous deep current measurement studies have interpreted lower-layer fluctuations as TRWs (Hamilton 1990; Hamilton et al., 2003; Hamilton in press, and the Exploratory Study measurements also have the same characteristics. Thus, motions were highly vertically coherent, were bottom intensified, and the principal major axes of the variance ellipses were at an angle to the local isobaths. The frequency content of the lower-layer currents are given by the kinetic energy spectra in variance preserving form, where equal area under the curve represent equal contributions to the KE (Figure 5-1). All the spectra show bottom intensification (the 2925 m level at L5 was within the frictional bottom boundary layer), however, the intensification was much greater between 1000 and 2000 m than below 2000 m. The high coherence of current fluctuations in preferred frequency bands allows the lower layer to be treated as a single entity. Therefore, the horizontal coherent structures were eventually investigated using a single record at each mooring From a consideration of spectra from dynamically comparable mooring, the Escarpment appears to have been a filter for longer period motions as well as an impediment to energy transmission into shallower water. As a consequence, periodicities of the fluctuations depended on the location of the records and both the east-west position and the position relative

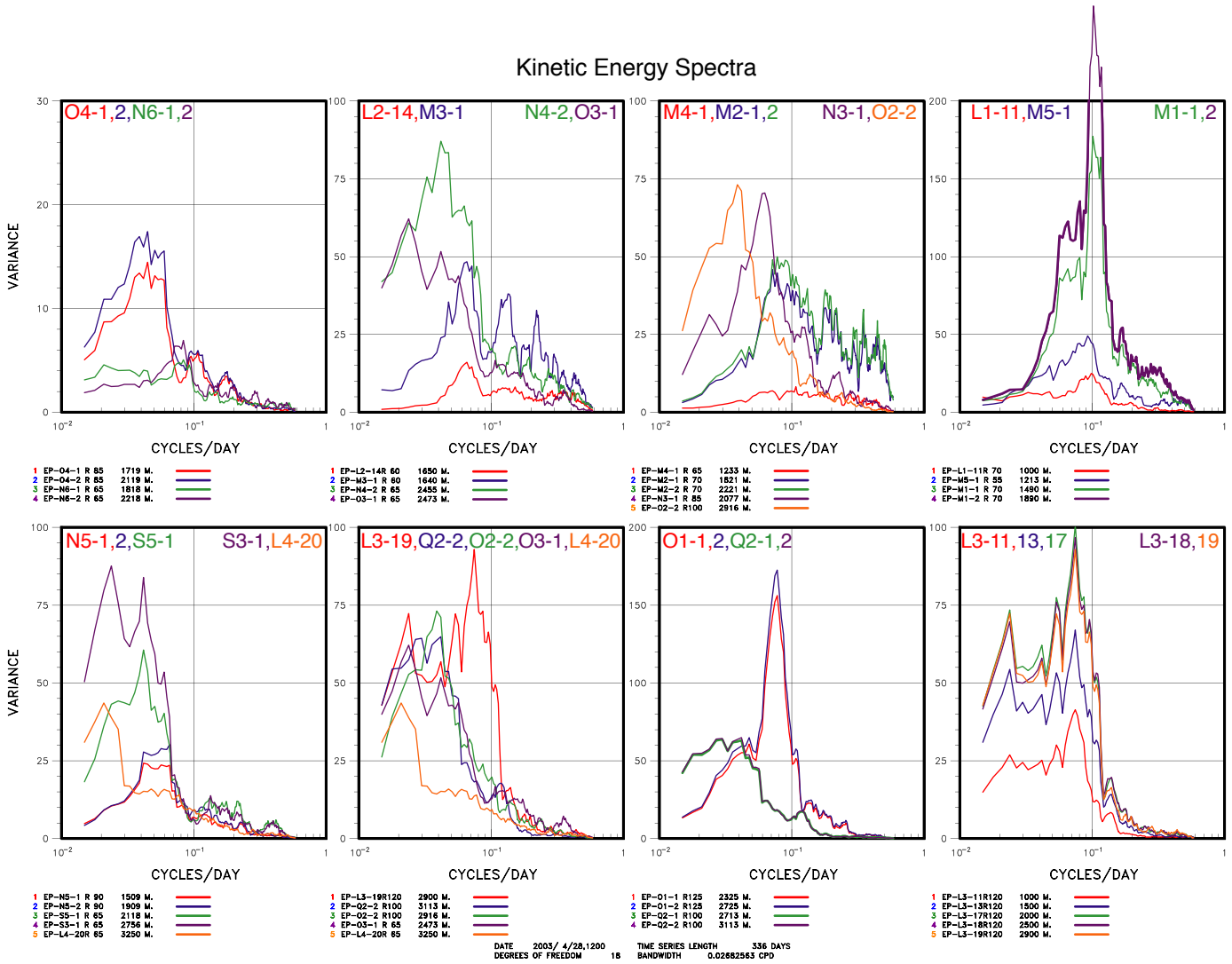

Figure 5-1. Kinetic energy spectra in variance preserving form for selected lower-layer 40-HLP current records. The plots group moorings in the same geographical vicinity and are arranged west to east (left to right) and north to south (top to bottom).

to the Escarpment were important. Except at the common mode frequency, the detided and detrended bottom-pressure anomalies measured by the PIES were directly related to the lower-layer currents through geostrophy. Therefore, the spectral content of the bottom pressure anomaly should be similar to that of the currents.

The complex spatial distribution of dominant periods argues for bottom motions being controlled by dispersive TRWs of different fundamental frequencies propagating along different characteristic paths that originate from undetermined LC processes further to the east. A translating eddy model in which cyclones and anticyclones translate southwestward along and adjacent to the Escarpment does not explain the inhomogeneous distribution of spectral peaks as it would produce similar time series of currents all along the Escarpment and thus similar spectra.

5.2.2 TRW Ray Tracing

The calculated ray path for the 61-day period TRW, initialized in the southeast corner of the array agrees reasonably well with the locations where the fluctuations had large amplitudes and were refracted away from the regions with small amplitudes (Figure 5-2). The backward ray trace indicates that the origin of the fluctuations may have been under the LC around 25.5°N. The 22-day ray paths are similar except that the path penetrates to a more northerly position on the Escarpment, which is consistent with there being relatively larger amplitudes at N4 compared to the southeast corner than occurred for the 62-day fluctuations. Both the transmitted and reflected paths were supported by the data if the transmitted path is strongly attenuated after crossing the Escarpment slope. The backward ray path fails or halts near 88.8°W, 25.2°N, suggesting a more local origin to the southeast of the array for these shorter period waves.

5.2.3 TRWs and Lagrangian Float Tracks

Particle displacements in linear TRWs are predicted to be rectilinear (Rhines 1970). Therefore, if deep-water motions were dominated by TRWs then water particle following devices such as RAFOS floats would be expected to oscillate with little long-term displacement. It is, of course, more complex than this as even linear TRWs have a broad range of periods, and close to the Escarpment, strong mean flows can generate large overall displacements. However, the general description of the RAFOS float trajectories have a number of instances where floats stayed in the same general vicinity for long intervals (several months), and the virtual float studies that use the bottom-velocity mapping products also indicate the dispersive wave-like nature of lower-layer flows.

Two case studies were used to argue qualitatively that TRWs and eddies can be the same physical process. The deep pressure maps were visually dominated by cyclonic and anticyclonic eddies. The quantitative demonstration that these deep fluctuations are TRWs was provided by the analyses that showed the currents of this same collection of features projected well onto TRW kinematics. Hence, it is appropriate to also view the eddies as constructed from a superposition of waves of different crossed wave vectors.

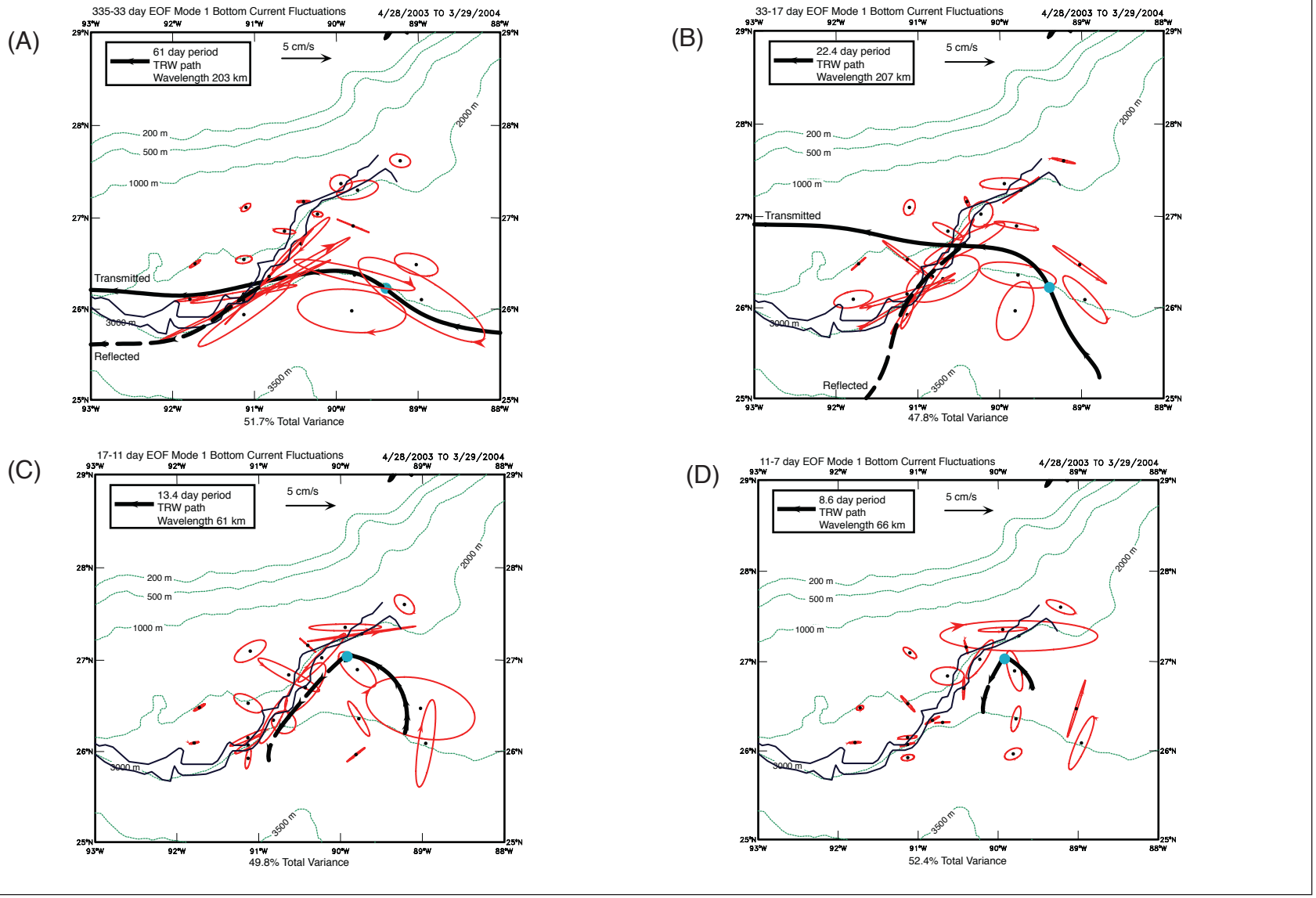

Figure 5-2. Path of TRWs traced backwards and forwards from the inital position given by the blue dot. Initial wavelength is calculated from the mode 1 EOF at the mooring nearest to the initial position. The dashed line assumes reflection of the wave by the escarpment. The mode 1 amplitude ellipses are are also shown. Arrowheads are at 5-day intervals.

It is clear that the central GOM is one of active east-west exchange. Although the predominant circulation in the deeper layers of the western basin (Sigsbee Plain, Mexico Basin) is cyclonic, the picture in the intermediate layers (1500 m, for example) is less clear. There is a tendency in the eastern basin to observe anticyclonic flow in the intermediate layer; however, the fact that the LC extended far to the north during much of the experiment may contribute to this. Also, there is not an even distribution of the floats, so statistics can be deceiving. For this reason, we have chosen not to try to present figures for quantities such as mean flows. Another clear feature of the large-scale flow pattern was the tendency for westward moving floats often to follow bathymetric contours and even converge towards the boundary.

Numerical (or "virtual") floats were used to examine circulation and eddies that move water and momentum across the study area, as well as to determine their dominant pathways. These numerical particles were advected by horizontal velocity fields obtained every 12 hours from the PIES analysis at the 1500 dbar pressure level. The virtual floats mimic the RAFOS float trajectories and characteristics, and show the same acceleration westward along the Escarpment in the presence of cyclones. Flows tend to be parallel to topography, except in the vicinity of eddies. The majority of the virtual floats are expelled from the domain within three months after deployment.

5.3 Upper and Lower Layer Interactions

Measurements of ocean currents in the GOM that span both upper and lower layers of the water column can provide some insight to linkages that may exist between two dynamically different environments. Typically, current patterns in the upper and lower layers are generally quite dissimilar reflecting differing processes controlling the observed circulation.

Strong upper-ocean circulation features were found to be potentially coupled with the deep circulation. Three classes of dynamical coupling were identified. In the simplest case, the upper-layer flow distorted the background flow field. Eddy Sargassum's deep thermocline presented an obstacle in the path of a deep cyclone and temporarily halted its westward propagation (Figure 5-3). The second category highlighted the more dynamical vertical coupling that results when propagating upper-ocean features stretch or squeeze the lower layer (Figure 5-4). The lower-layer response to vortex stretching/squeezing requires the acquisition of positive/negative relative vorticity to balance the changes in thickness in order to conserve total potential vorticity. Two cases revealed the joint propagation in the upper and lower layers of a cyclone pair and anticyclone pair. In each case, the lower-layer eddy led the upper-layer eddy in a vertically tilted fashion characteristic of coupled propagation. Finally, a case studied presented observations consistent with baroclinic instability, in which the phase of this vertical tilt and the wavelength lead to joint growth of the upper and lower layer perturbations (Figure 5-5). A meander crest within the LC jointly spun up with a deep anticyclone that was offset to the west and slightly north of the growing crest.

Evaluating a time sequence of overlaid images of float trajectories and satellite SSH data shows that in most cases and areas very little correlation existed between what is seen in the surface elevation fields and in the float tracks. The only significant exception appears to be late in the record (March-May 2004) under the LC as it extended into the GOM. In this case, several floats

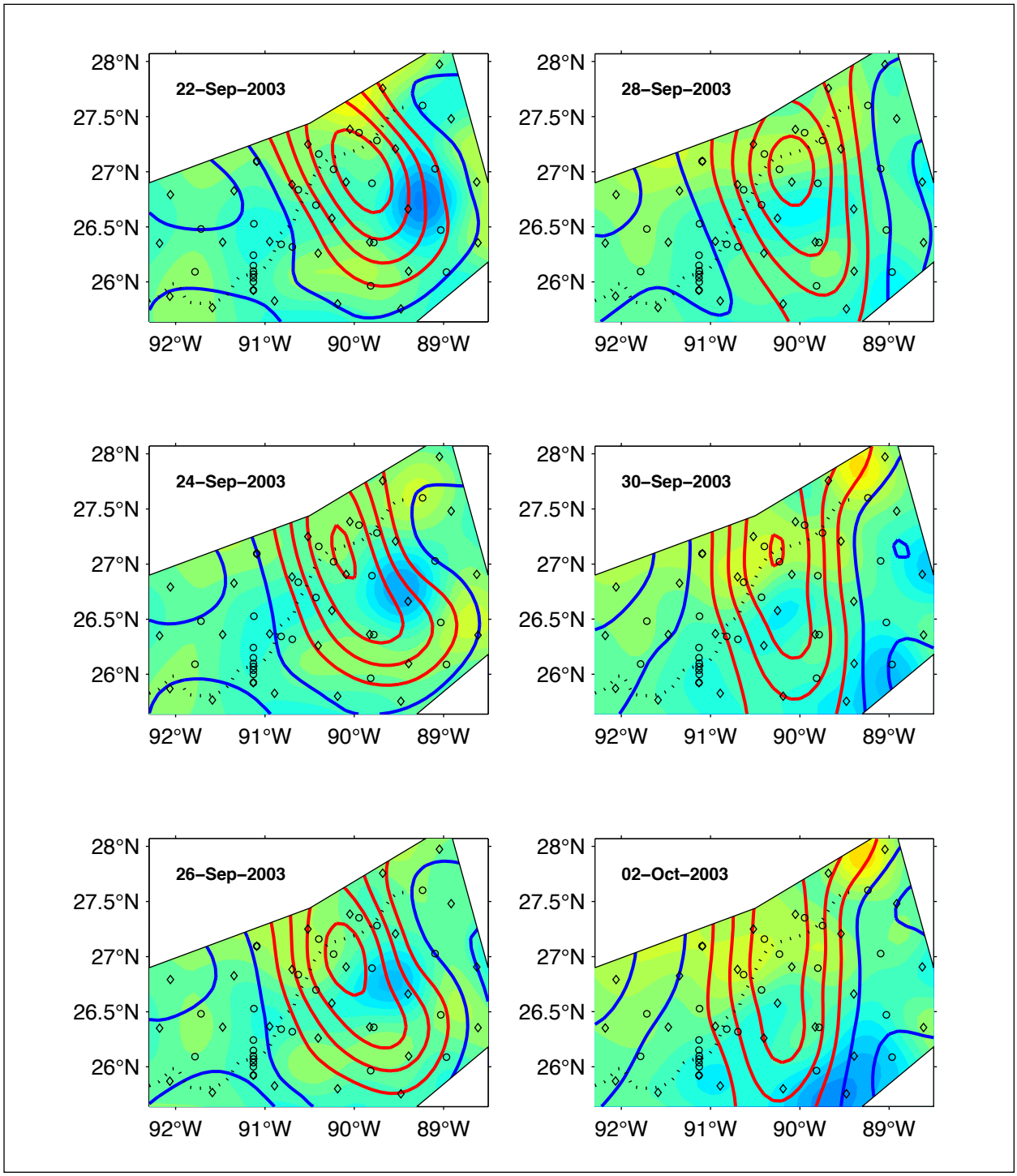

Figure 5-3. Case study: Upper-layer circulation halts deep-eddy propagation [22 Sept - 02 Oct. 2003]. Maps of surface streamfunction (bold contour lines) superimposed upon shaded contours of 1500-m dpeth pressure for six separate days. The sequence begins with the top left panel. The dotted line denotes the center of the Sigsbee Escarpment. PIES sites indicated by diamonds; current meter moorings by circles.

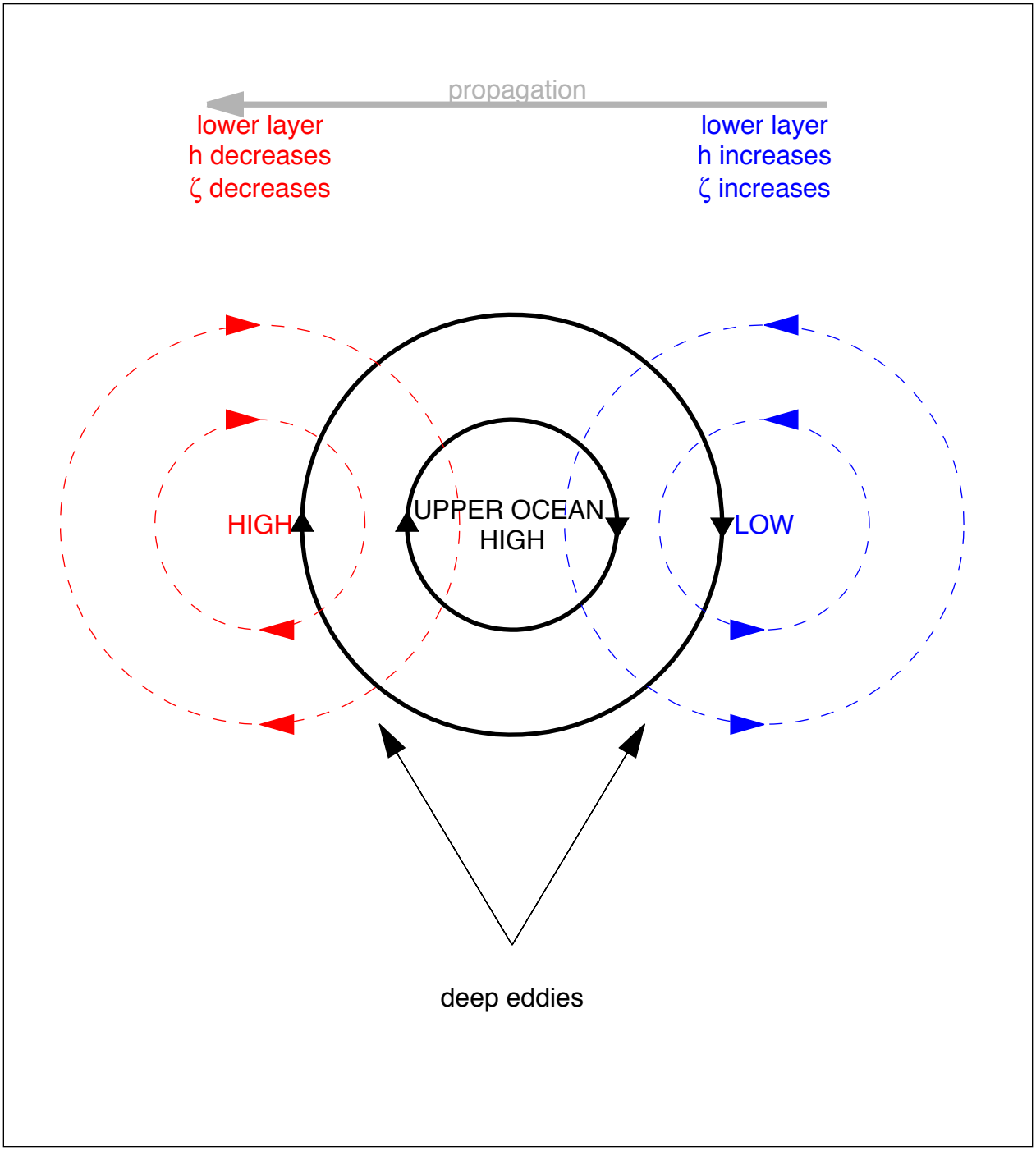

Figure 5-4. Schematic representation of propagating upper-ocean anticyclone (solid black) and leading lower-layer anticyclone (dashed red) and trailing lower-layer cyclone (dashed blue).

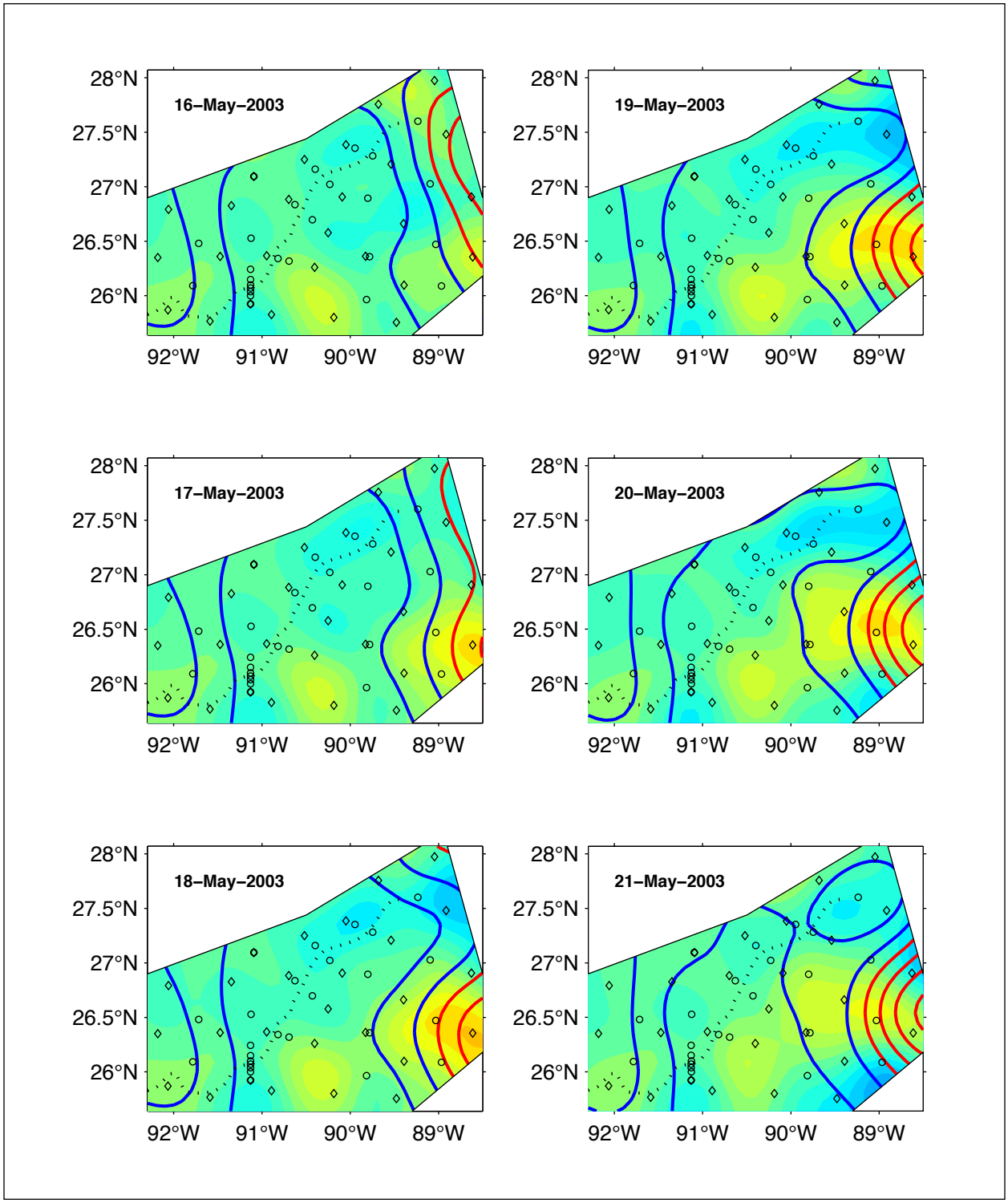

Figure 5-5. Case study: Baroclinic instability [16-21 May 2003]. Maps of surface streamfunction (bold contour lines) superimposed upon shaded contours of 1500-m depth pressure for six separate days. The sequence begins with the top left panel. The dotted line denotes the center of the Sigsbee Escarpment. PIES sites are indicated by diamonds; current meter mooring sites indicated by circles

at 1500 m (poor coverage was available from the shallow floats at 1000 m) were seen to retreat northward into the Gulf as the LC extended. Several floats were observed to become trapped in a "saddle point" between the main part of the LC and an eddy that separated to the north. Several of these floats also were observed to follow along the SSH height contours of the LC for fairly short time intervals, but then diverged from them and crossed contours. During this time there was little relation between the float tracks in the western GOM and the SSH fields.

6.0 HIGH-FREQUENCY VARIABILITY

Previous studies of high-frequency currents in the deep GOM have shown them to be dominated by inertial oscillations. Near-inertial currents are internal waves with periods near $2\pi/f$, where f is the Coriolis parameter. Motions are characterized by a clockwise rotating vector (viewed from above), and the internal wave has upward phase propagation and a downward component of group velocity. Near-inertial currents are usually generated by changing surface winds that often occur in conjuntion with storms. Rapidly moving hurricanes can generate large inertial wakes in deep water that can persist for many days to as long as several weeks after the tropical storm had passed (Brooks, 1984; Shay and Elsberry, 1987; Hamilton et al., 2000). Though surface winds are thought to be the major source of inertial energy, inertial oscillations can also be generated by processes of geostrophic adjustment and thus may be generated by large-scale flow interactions such as eddy – eddy and eddy – topography interactions. Although evidence of these interaction-based processes is difficult to discern in current data, many observations of energetic inertial oscillations at considerable depths below the wind-forced surface layer have been observed.

Inertial oscillations are intermittent, narrow-band, clockwise rotary current fluctuations. The main source is surface wind fluctuations, though eddy instability processes involving geostrophic adjustment may also be a source in certain circumstances. The use of ADCP current profilers in the upper part of the water column on the tall moorings allows the characterization of inertial oscillation velocities in both space and time.

Local inertial periods ($2\pi/f$) in the study region range from 25.9 hours at L1 (NE tall mooring) to 27.4 hours at L4 (SW tall mooring). These periods overlap those of the dominant diurnal tide in the GOM. As a consequence, it is almost impossible to separate diurnal tidal from inertial motions. However, the barotropic diurnal tidal current in water depths greater than 1000 m has small amplitudes of a few $cm \cdot s^{-1}$ and therefore can be safely neglected.

6.1 Eddy Sargassum Inertial Currents

An initial investigation of high-frequency current oscillations in the upper-layer above 400 m showed that unusually large currents occurred at L1 when Eddy Sargassum was over the site. The inertial oscillations during this event are shown in Figure 6-1, where the velocity components have been high-passed filtered with a filter having a cut-off period of 50 hours. The north or V-component leads the east or U-component by 1/4 (90°) period and has a similar magnitude. This is the signature of a clockwise almost circular rotating current. The event emerged from similar shorter period, lower-amplitude oscillations, grew and then decayed over a period of about 25 days. Maximum amplitudes occurred at a depth of ~168 to 200-m on August 25, with lesser currents above and below.

Inertial peaks in the spectra, for a 36-day period centered on August 25, 2003, are shown in Figure 6-2. The center frequency was about 0.8 cpd or 13% less than the local inertial period. This corresponds to a period of about 30 hours and thus a latitude of ~24°N if the waves were generated in a quiescent ocean. The spectra also show the increase in variance at 200 m compared with near-surface (40 m) and deeper (300 m) depths. Figure 6-2 also shows 36-day

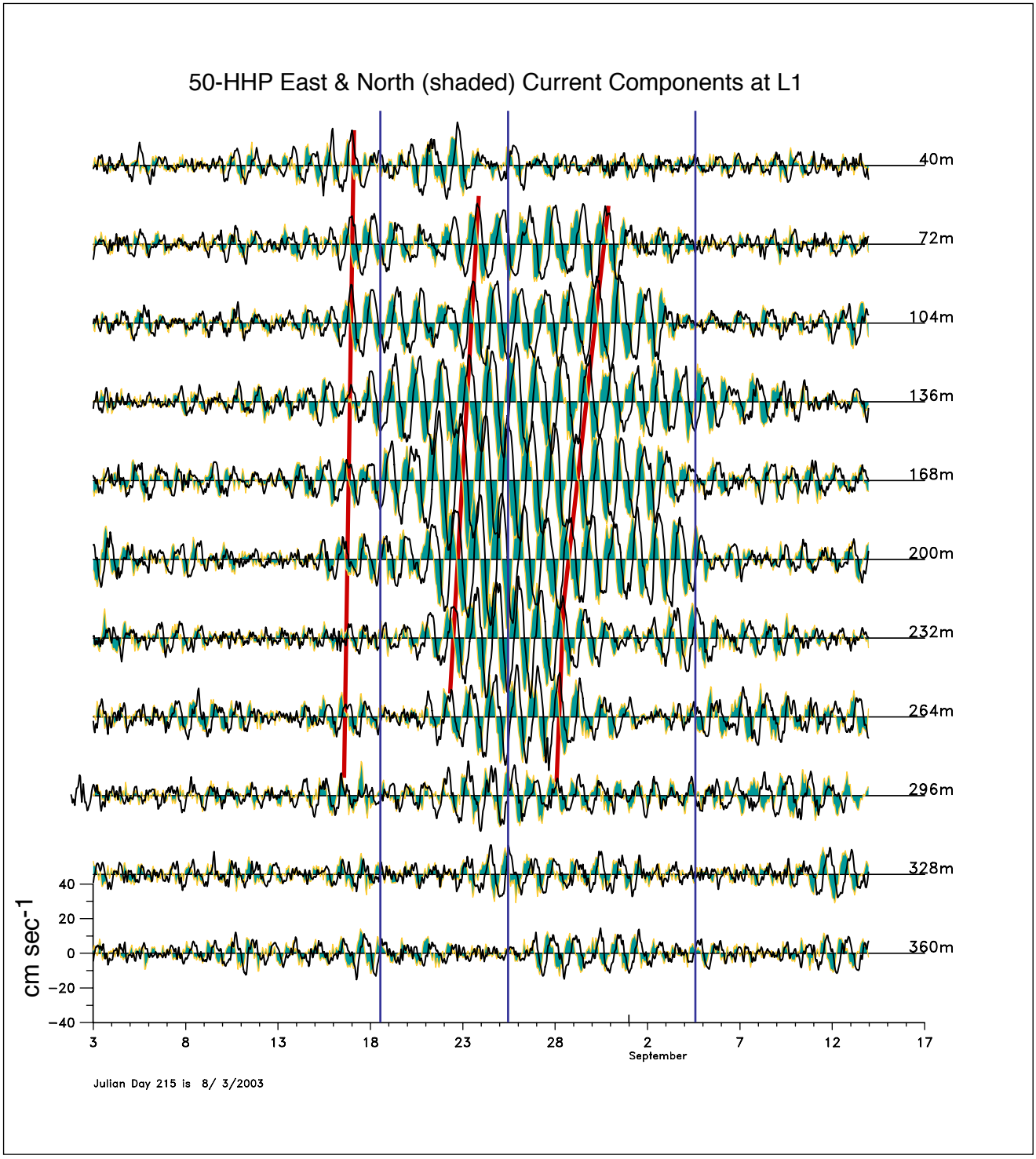

Figure 6-1. Inertial currents from the upper-most ADCP at L1 during the passage of Eddy Sargassum. Current records have been 50-HHP filtered. East (U) component is solid, and north (V) component is blue shaded. Red lines show approximate propagation of V-component peaks. Blue lines mark times discussed in the text.

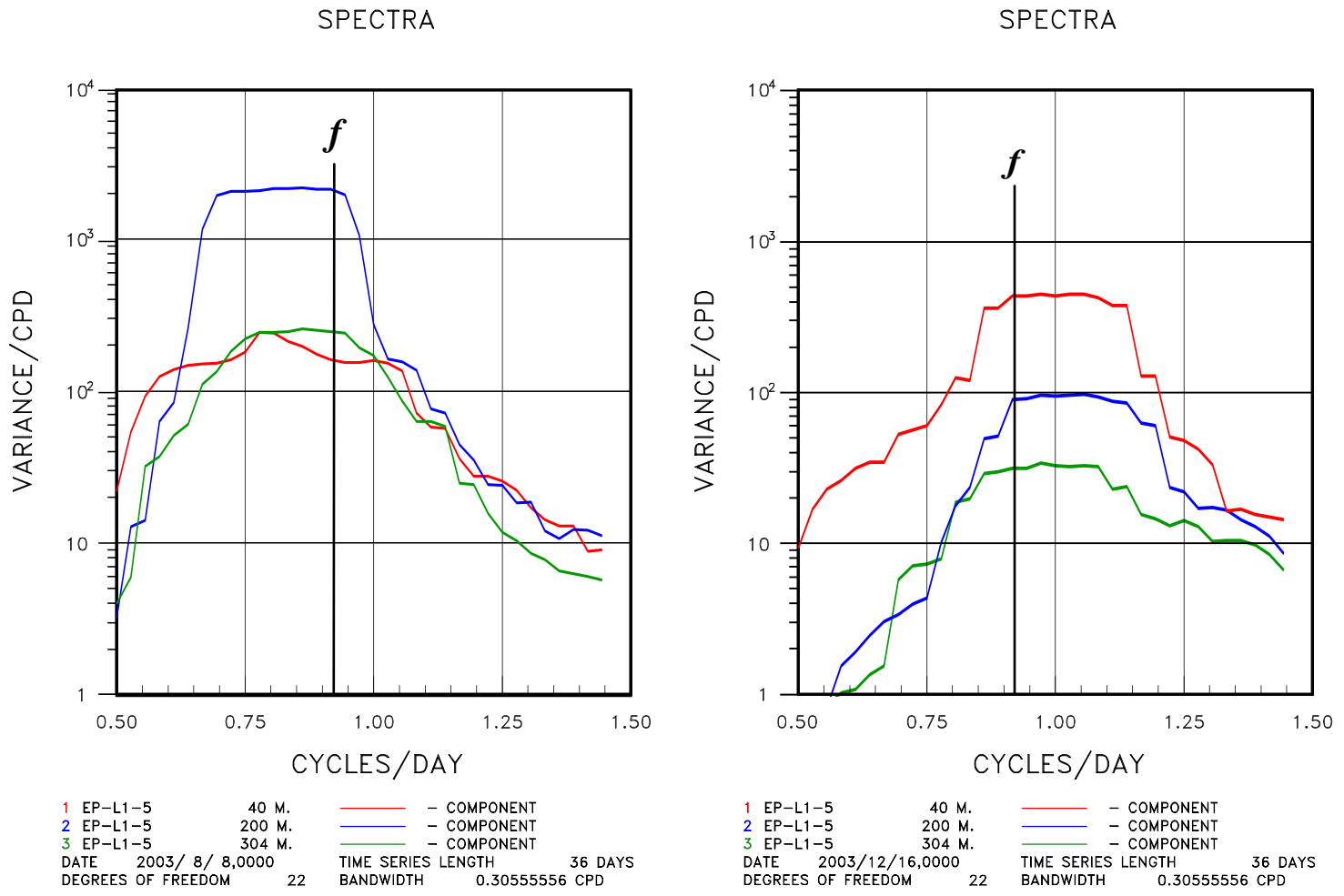

Figure 6-2. Clockwise component of rotary spectra at the indicated depths at L1 for 36-day intervals. Left panel: August 2003 eddy Sargassum event. Right panel: Winter storm event. Local inertial frequency (*f*) is indicated.

spectra from a more typical interval at L1 for the winter 2003-4. The latter show a consistent decrease with depth.

From a frequency-domain EOF analysis of the inertial oscillations at both periods, two modes were significant and accounted for greater than 75% of the total variance in the bands centered about the peak frequencies of 0.8 and 1.0 cpd, for the eddy and winter, respectively. These data suggest that at this time Eddy Sargassum contained two wave trains of similar period that had different trapping depths. This could be because the vertical shapes of the modes resulted from waves generated at different times in the past or they could have had slightly different frequencies not resolved by the band averaging of the analysis. The vertical distribution of inertial amplitudes and phases in the winter case in the absence of an eddy affecting the mooring also indicates two modes. The implications of this are that the vertical distribution of wind-generated inertial currents at any given time may have had more than one source.

Data from this study show that inertial currents were affected by the presence of eddys and eddy-eddy interaction affected these inertial currents and produced complex reconstructions of currents at a fixed measurement site as the eddy translated, rotated and interacted with the ocean environment. These interactions influenced the local inertial period and, in conjunction with changes in latitude of the eddy, can result in subinertial waves escaping from the LCE center.

Contrasting the results for L1 and L5 when the eddy was similarly situated relative to the moorings, indicates that the exceptionally large amplitude (~ 40 $cm \cdot s^{-1}$) inertial oscillations, with a frequency substantially lower than local f, short vertical wavelengths and confined to the upper 300 m, had essentially disappeared during the month-long passage from L1 to L5. There is a possibility that the amplitude maximum at 600 m in October was a remnant of this activity with some of the inertial waves escaping confinement by the eddy's vorticity, and propagating down into the water column as the eddy translated southwestward along the Escarpment. However, this deep event at L5 could have propagated vertically and horizontally from outside the eddy to the lower part of the eddy where the low-frequency currents and relative vorticity were small. Thus, its occurrence could be coincidence and just part of the complex fields of inertial oscillations that are ubiquitous in the upper layers of the GOM. The source of the exceptional inertial currents at L1 is unknown, but it is speculated that during the long period when the eddy was still attached to the LC and was relatively stationary (see Section 4) inertial energy could have accumulated from frequent favorable wind events. Another possibility is that the detachment process or other eddy-eddy interaction, converted some of the ring's low-frequency energy to inertial oscillations through geostrophic adjustment processes. It seems fairly clear that these trapped inertial currents dissipated fairly rapidly after their occurrence at L1.

6.2 Inertial Oscillations due to Forcing at the Ocean Surface

Some documented inertial (narrow-band, clockwise rotary) currents result from wind/pressure events at the ocean surface. During this study, two hurricanes and two tropical storms passed over or close to the array in the summer of 2003. The storm tracks, obtained from the National Hurricane Center's analysis, are given in Figure 6-3 and are also identified in the wind records. The storm summaries are given in Table 6-1. Tropical storms Henri (September 3-8) and Larry

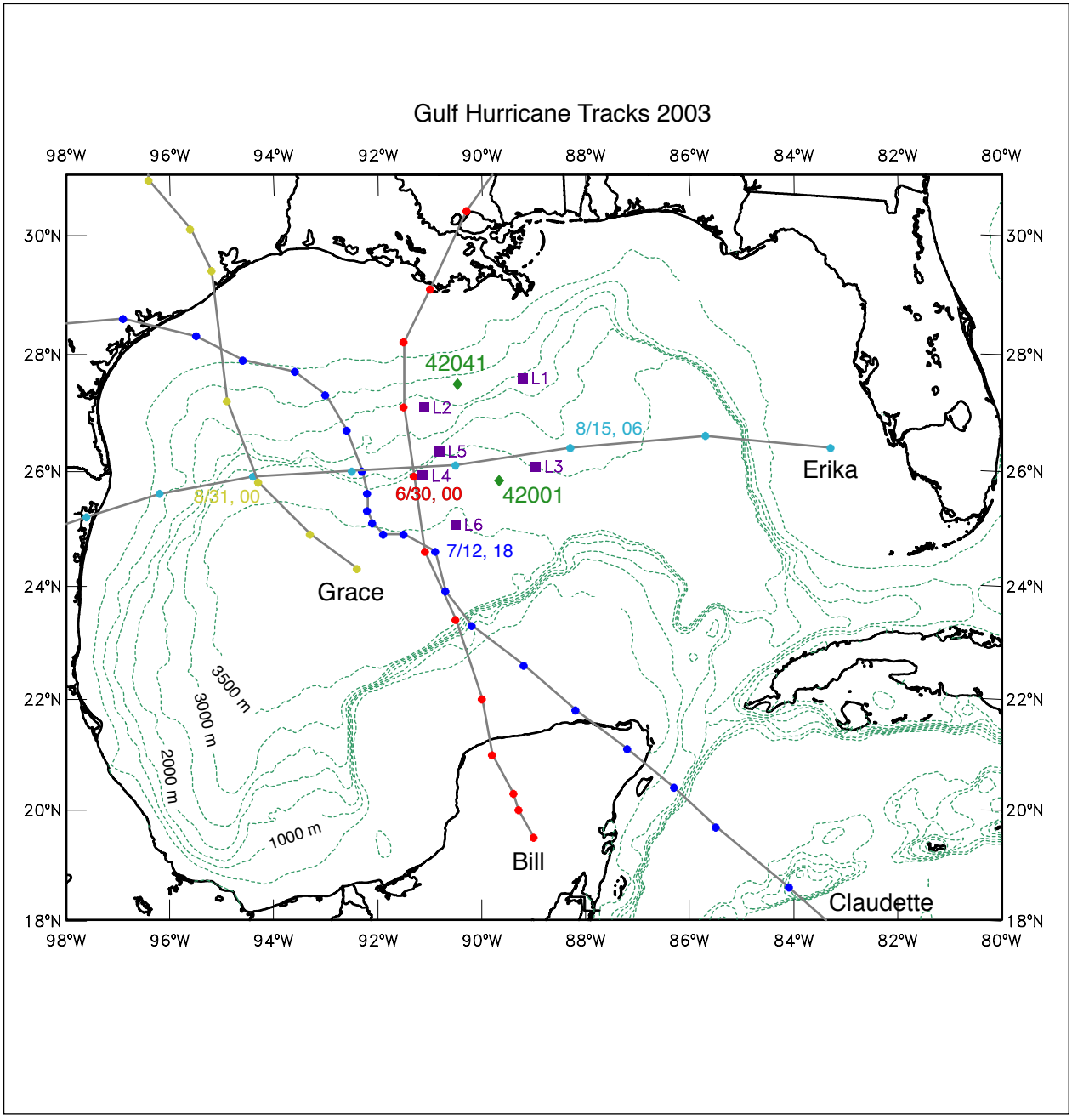

Figure 6-3. Tropical storm and hurricane tracks for the Gulf of Mexico in 2003. The center low pressure positions are given by the dots at 6-hour intervals. Date and time (GMT) of a close approach to the array is noted for each track, and the positions of the tall moorings (squares) and NDBC buoys (diamonds) are also shown.

(October 1-6) also occurred over the eastern Gulf and the Bay of Campeche, respectively, but had little or no influence on winds over the array.

Strong inertial oscillations are usually observed on the right hand side of the track of the central low pressure of a rapidly moving tropical depression. All the tracks, except Erika, passed to the west of the measurement array (Figure 6-3), and Erika's east to west track passed almost directly over L3 and L4. It is, however, difficult to see a consistent response of large amplitude oscillations at the various moorings to the passage of these storms

Table 6-1

Gulf of Mexico Hurricanes during the Study

Name	Dates	Maximum Sustained Winds ($m \cdot s^{-1}$)
Tropical Storm Bill	June 29 – July 2	25
Hurricane Claudette	July 8 – July 17	37
Hurricane Erika	August 14 – August 17	32
Tropical Storm Grace	August 30 – September 2	17

Despite the great complexity of the inertial-internal wave field, there is some evidence that activity was greater when a site was within a warm-core eddy and this increase was probably caused by trapping of the energy by the negative relative vorticity field. The observed energy is then the result of the cumulative effects of wind forcing and trapping.

RAFOS float trajectories did not provide a good observational basis for evaluating inertial currents. The accuracy and frequency of the RAFOS float position estimation were ± 500 m and 3 times per day, respectively. The approximate radius of an inertial circle at these latitudes (26.5°N) for a velocity of 10 $cm \cdot s^{-1}$ is about 1.5 km. Consequently, these drifter trajectories could not well resolve deeper inertial currents unless they were extremely energetic.

7.0 SUMMARY AND RECOMMENDATIONS

7.1 Summary of Study Results

The Gulf-wide, upper-ocean circulation during the Exploratory Study field measurements was dominated by two strong LC events, Eddies Sargassum and Titanic, that resulted in strong LC and LCE circulation in and around the study region throughout the program. Cyclonic circulation that is typically associated with strong LC intrusions and eddy separation events was also present. The summary of the historical record of remote sensing observations of LC intrusion and LCE detachment and separation events described in Chapter 3 were used to place the program field interval into an historical context. While it may be simplistic to characterize the Gulf-wide oceanographic conditions impacting the study region as unique during the Exploratory Study, the observed LC variability resulted in a range and duration of oceanographic conditions that may not typically be observed over a one-year time set of measurement. This was confirmed quantitatively using the historical record of altimeter derived LC and LCE metrics. The Eddy Sargassum intrusion was the most northerly intrusion event observed in the altimetric record to date and shed a LCE that passed directly through the Exploratory array, interacting with the Sigsbee Escarpment along its entire trajectory. The two LCEs observed during the program time period, Sargassum and Titanic, both momentarily detached from the LC. If these eddies had not reattached to the LC they would have ranked near the top of all LCEs in terms of eddy size and intensity. While we had the good fortune to observe a great range of energetic LC activity during the yearlong program, the conditions were not so atypical that the average LC behavior over the one-year time period, as measured by the mean LC metric statistics, differed remarkable from the long-term average.

7.1.1 Upper Layer

The LC and associated eddies, both anticyclonic and cyclonic, dominated the upper-layer circulation in and around the study region during the field measurements. Dynamical interpretation of this upper-layer circulation was difficult because of the complexity the eddy interactions – an eddy field that can be best characterized as an energetic nonlinear flow, at least during the first half of the program time period. A shielded vortex instability was proposed as a strawman framework for dynamically interpreting the Eddy Sargassum LC/LCE vortex system that impacted the study region early in the measurements. The deepening of the upper layer and the peripheral LC cyclones associated with this instability process provide physical forcing mechanisms at frequencies and wavelengths commensurate with the time and space scales associated with the forcing of the most energetic TRWs and upper-layer baroclinic eddies/waves observed. Upper-lower layer coupling through baroclinic instabilities likely contributed to the twisting and tilting of the Sargassum LC/LCE vortex system. The limited region of full water column information, however, makes identifying baroclinic instabilities within the LC/LCE system difficult since most of the instability likely occurred outside the study region.

Energetic (amplitude ~30 to 40 $cm \cdot s^{-1}$) inertial oscillations were observed at L1, at thermocline depths (150 to 250 m), in the core of Eddy Sargassum. The peak period was longer than local f, the Coriolis parameter, and therefore, it was surmised that the inertial energy was trapped by the negative relative vorticity of the eddy and was possibly the result of energetic wind events (some

from tropical storms) that occurred earlier while the eddy was further south and still attached to the LC. The summer of 2003 had an active hurricane season with two tropical storms and two hurricanes passing close to or through the array. The inertial response to these events was observed at most of the tall moorings, with more energetic fluctuations propagating down from the surface. In general the distribution of inertial energy in the upper part of the water column was complex both in time and with depth and was sometimes difficult to relate to local wind events.

7.1.2 Lower Layer

Deep energetic currents, below 1000 m, were typically associated with eddies observed in the deep pressure fields that may be interpreted as a field of dispersive TRWs. The dispersive nature of the bottom circulations, and the relatively continuous character of the current fluctuations confirm the fundamentally wave-like behavior of the deep flows in the study region. Once west of 89°W, deep eddies typically translated northwest until they encountered the Escarpment, where their behavior depended upon the sense of eddy rotation. Strong cyclones approached the Escarpment and deflected left in the direction corresponding to topographic westward. In contrast, anticyclones encountering the Escarpment typically stalled and decayed rather than propagate away.

Mean and fluctuating flows had distributions that were inhomogeneous in both magnitude and frequency content from deep to shallow and east to west along the slope. The strongest fluctuations (~60 $cm \cdot s^{-1}$) were found below the Escarpment in the east and have the characteristics of TRWs, presumably generated by the LC, that propagate westward towards the steep slope. The Sigsbee Escarpment effectively barred these energetic currents from penetrating into shallower water, and also trapped short period (~10 days) waves in the east of the study area. Longer period, 30 to 60-day, waves were refracted and propagated back southwest towards deeper water. Closely spaced measurements across the Escarpment at ~91°W showed a strong mean jet-like flow centered over the steepest slope, with maximum mean velocity over 12 months of 13 $cm \cdot s^{-1}$ directed towards the southwest. A number of deep float tracks also had the characteristics of TRW's in that they oscillated, with an across-isobath component, over a limited area of the abyssal plain for periods of several months. Near the Escarpment, float tracks tended to rapidly translate along the steep bathymetry into the western GOM.

7.1.3 Upper-Lower Layer Coupling

Strong upper-ocean circulation features were found to be coupled with the deep circulation. Three classes of dynamical coupling were considered. In the simplest case, the upper-layer flow distorted the background flow field. Eddy Sargassum's deep thermocline presented an obstacle in the path of a deep cyclone and temporarily halted its westward propagation. The second category highlighted the more dynamical vertical coupling that results when propagating upper-ocean features stretch or squeeze the lower layer. The lower-layer response to vortex stretching/squeezing requires the acquisition of positive/negative relative vorticity to balance the changes in thickness and conserve total potential vorticity. Finally, a case study presented

observations consistent with baroclinic instability, in which the phase of this vertical tilt and the wavelength led to joint growth of the upper and lower layer perturbations.

7.1.4 PIES – Altimeter Comparison

The study of the altimeter sampling using the PIES SSH data showed that 87% to 99% of the subinertial period SSH variability in the Exploratory Study region is unaliased by the approximately 10-day Topex/Posiden repeat-period sampling; however, there can be significant aliasing of the GOM SSH signal in satellite altimetry even with the dominance of the longer period baroclinic signals in the deepwater of the Gulf. This is especially true for 35-day sampling. The degree to which this affected the space/time interpolated maps of SSH needs to be investigated in more detail. It also is unclear whether the weak surface signature of TWRs can be mapped effectively using satellite altimetry given the presence of the strong baroclinic SSH and the difficulties associated with aliasing of the signal.

The Colorado Center for Astrophysical Research (CCAR) mesoscale SSH gridded-altimeter data field that was compared with the coincident PIES SSH. The CCAR/PIES SSH correlation were good with an overall mean correlation of 82%. Lowest correlations were found above the Escarpment and along the western edge of the study array. SSH slopes between PIES stations were also compared to the coincident slopes calculated from the CCAR mesoscale product. The overall mean correlation was 80%.

7.1.5 Deep Float Trajectories

Floats released in the lower layer of the central northern GOM showed evidence of east or west exchange. However, trajectories once the floats moved out of the general deployment area exhibited patterns dependent on whether they moved to the west or the east. Most floats that moved to the east tended to display more eddy-like motions and did not show a strong correlation with upper layer motions inferred from other (e.g. altimetric) data. Floats that moved to the west toward the Sigsbee Basin tended to converge toward the steeper slope, accelerated, and followed narrow paths westward and then southward along the boundary. A few of these floats eventually were entrained in deep eddies along the western boundary and moved into deeper parts of the basin.

7.2 Hypotheses

One item in the overall study objectives, were eight hypotheses to be evaluated using the results and insights developed in this study. Presented below are those hypotheses with an associated response.

H1: Currents shallower than 800 m are dynamically uncoupled from currents at depths greater than about 1,000 m.

Although some dynamical linkage of upper and lower layers have been postulated based on a diverse evidence set in this report, there was not conclusive evidence of the importance and nature of this linkage. The argument remains that lower layer dynamics need to be driven by some source and the most likely is a link to the upper layer events

such as the LC or a LCE. This link can not be easily deciphered, but measurements similar to those in this study, but underneath and to the west of the LC may provide more information on upper-lower layer relationships that are active in the present study area.

H2: Rare mid-water jets occur in areas of eddy-eddy interactions.

There was no substantial evidence of mid-water jets at the various full depth moorings, so this hypotheses cannot be accepted.

H3: Currents in water depths greater than 1,000 m never show a large vertical gradient of velocity.

Currents in the lower layer are strongly barotropic and hence have weak vertical gradients. Generally, the depth having the lowest velocity occurs in the transition region where upper layer dynamics diminish in importance to local circulation patterns and the lower layer patterns begin to dominate. From this transition zone to the local bottom, the relative magnitude of currents tends to increase. Thus, this hypothesis would be accepted.

H4: Deepwater parameters measured in areas dominated by cyclones/anticyclones of scales of 50-100 km are not different from areas not dominated by cyclones/anticyclones of 50-100 km.

A definitive response to this hypothesis is not presently possible. In the present study the presence and path of 50-100 km cyclonic/anticylonic eddies was greatly affected by the position of the LC and path of LCE. Clearly, these locations and positions were major factors affecting eddy development and movement.

H5: There are no differences in the occurrence and/or intensity of near bottom currents near steep bathymetric gradients and areas of small bathymetric gradients**.**

Results showed that near-bottom currents tend to be greater in the vicinity of steeper bathymetry in the study area. Based on this studies measurements, this hypothesis would be rejected.

H6: The characteristics of topographic Rossby waves change from east to west in the Gulf of Mexico because of changes in bottom slopes and frictional dissipation that causes the TRW's to reflect, trap and dissipate by wave breaking**.**

Results indicated that the previously postulated transition from short to longer period TRWs in going from east to west over the GOM basin was true over the measurement domain of this study. A factor in this could have been the role of bottom slope in governing the characteristics of TRWs supported by regional bathymetric conditions.

H7: Circulation below 1,000 m in the Gulf of Mexico is dominated by cyclone/anticyclone pairs and is fundamentally cyclonic.

The role or presence of lower-layer cyclones/anticyclone pairs is not well resolved. The reader is also refered to the discussion of the resolving of eddies vs. wave motions and that they can be different forms of the same thing, see section 7.1.2 where it is stated that "deep eddies may be interpreted as resulting from a field of dispersive TRWs. Thus, the frequency domain EOF analysis of TRWs in Section 5 can be regarded as analogous to a

frequency and wavenumber decomposition of an eddy field." There did appear to be a persistent cyclonic flow along the Sigsbee Escarpment that intensified toward the west.

H8: Storm generated inertial oscillations trigger resonant phenomena that propagates into deepwater.

At the tall moorings, inertial oscillations were observed and related to tropical storms. These single and multiple periodic current patterns propagated vertically into deeper water, although given the separation of tall moorings there was no clear evidence of the same but evolved wave field arriving at two moorings. It was difficult to specifically relate all inertial oscillations to meteorological events. It is possible that some inertial patterns may have resulted from geostrophic adjustment (this is when the pressure field and the velocity field are changing to maintain a balance of forces) due to eddies interacting with bathymetry.

7.3 Assessment of Measurement Program

7.3.1 Introduction

The Exploratory Study was designed with three complimentary components: the mapping array of PIES and current meter moorings, the deep Lagrangian drifters, and remote sensing by altimeters and SST/Ocean color. Principal aims of the design were to observe, map, and track the four dimensional (x,y,z,t) dynamical structure of the circulation in both the upper and deep layers throughout a substantial region of the northern Gulf slope. This information is needed to reveal and understand the important vertical coupling by which deep and upper eddies affect circulation and eddies in the opposite layer. This goal was achievable at much less cost than by deploying a similar array of full depth current meter moorings. By necessity, the mapping is restricted to subinertial period geostrophic motions associated with eddies and topographic Rossby waves. The choice of the lateral separation between measurement sites took advantage of previous observations which had demonstrated that the predominant large scale low frequency currents are geostrophic, in the upper eddies and in the deep topographic Rossby waves and eddies. Finer spaced observations were required in the deep layer near steep topography such as Sigsbee Escarpment. Also finer spaced upper observations would be appropriate in the future to resolve smaller scale, upper-layer motions such as rapidly translating peripheral cyclones on the LC or LCE fronts. A limited number of full-depth moorings (including moorings deployed by LSU (Nan Walker) and CICESE (Antoine Badan)) were included in the array so that some aspects of higher frequency motions (principally inertial oscillations) and ageostrophic flows could be examined. The PIES/mooring array was highly successful in resolving the temperature, salinity, current and dynamic height structures of upper layer eddies and also the smaller length scales of the currents and pressure fields of the deep TRWs and eddies.

A unique aspect of the array design was placement of PIES on or near altimeter ground tracks so that the satellite measured SSH can be directly compared with PIES derived dynamic heights and bottom pressure. Thus, the contribution of lower-layer eddies and TRWs to SSH could be assessed. The barotropic component of SSH was 5 to 10% of the total signal, in rms average, with peak displacements of 20 cm, compared to about 80 cm total SSH range across an LCE. It is noted that most numerical models assimilate SSH from altimeters purely as a baroclinic signal; however, PIES measurements could provide useful information to develop techniques for

assimilating both the baroclinic and barotropic components of SSH derived from altimeter observations. The SSH maps from the altimeters also provided a Gulf-wide perspective within which the more highly resolved and smaller scale PIES array was placed. Thus, the LC and eddies were tracked before and after they directly affected the array.

Drifters provided the other Gulfwide perspective for the lower layer. The use of RAFOS drifters in the Exploratory Study was a first for the GOM. The RAFOS tracks provided new results for the deep water in that large displacements, that imply strong mean flows, tended to occur in the vicinity of steep slopes such as the Sigsbee Escarpment. However, in many cases RAFOS and PALFOS floats oscillated around the same relatively small region for several months at a time. The latter behavior for deeper RAFOS floats is consistent with deep motions being dominated by TRWs, rather than translating eddies. TRWs, at small linear amplitudes, do not transport mass or relative vorticity. There also appears to be weak exchange between the eastern and western basins as yet unseen in some modeling results and raises questions on the flushing times for renewal of deepwater in the western basin that have not yet been explored. There was also almost no relationship of the deep float tracks to the upper-layer eddy circulations given by the altimeter SSH. Within the mapping array, the float tracks were consistent with geostrophic currents derived from the PIES and current meters as well as with the wave-like dispersive nature of the lower layer flow field.

7.3.2 Resolution

A PIES array with mean nominal spacing of 60 km resolved the temperature, density, and velocity structure of the LC, LCE (Sargassum and Titanic) and several cyclonic features. Mapping accuracy was consistent with the correlation properties of the observed mesoscale features. Closer horizontal resolution would be required to resolve more fully the strong cyclonic frontal cyclones that exist along the periphery of the LC, typically between 89° and 86°W.

The deep circulation, TRWs, and eddies were observed by deep current meters and bottom pressure recorders, which are needed in combination to resolve the somewhat smaller lateral scales associated with these deep processes. The horizontal resolution was effective in the moderately-sloped topography away from the Sigsbee Escarpment. One array of current meters (called Array-S) spanned the Sigsbee Escarpment near 91°W, with very close spacing (5 sites spaced ~4 km) across the steep bathymetry, which revealed deep jet-like flows narrowly-focused along the steep isobaths. The location for the S-Array was well chosen to observe strong currents, because deep eddies commonly paused nearby contributing their strong currents to the S-Array records. The question naturally arises, how typical the 91°W location is of other locations along the Sigsbee Escarpment? Measurements in this and earlier programs near 90°W were at the base of the Escarpment. High currents were observed here (90°W) but it is not known whether current fluctuations or mean flows increased over the middle of the slope, as were observed at the S-section (91°W). The Sigsbee Escarpment zigzags WSW, alternating between segments that trend nearly-westward and others that trend SSW; an important clue to understand the deep jet dynamics may be offered by closely-resolved observations like the S-Array, but with better vertical coverage, on approximately 4 short transects between about 90°W and 91°W.

7.3.3 Duration

The Exploratory Study was fortunate to capture the effects of Eddy Sargassum, through a duration spanning most of its influence upon the study area, from its formation and the radiation of numerous energetic deep eddies, through its complete passage and associated events of vertical-coupling. Eddy Titanic formed and passed mainly to the south, producing less influence upon currents in the Study Array, followed by ~3 months of relatively weak upper and deep currents.

If the objective was to estimate the temporal-mean currents with statistical significance in the upper or the deep regions of the Exploratory Study, the duration of the study would have to be 2-3 times longer. A question for a future study is, how typical were the currents associated with Eddy Sargassum, and how similar or different the currents would be during the passage of another event like Eddy Sargassum? To address this question will require more observations of at least a similar duration.

7.3.4 Spatial Extent

A future experiment of larger spatial extent in all directions would help in understanding the propagation and impact of LCEs. It would be particularly valuable for observations to simultaneously span further east across the LC to study the forcing and radiation of deep eddies and to understand and predict the pinch-off process of a LCE. In evaluating this program, it is pertinent to bear in mind that Eddy Sargassum was the farthest-north LCE to form and pass through this region in the past several years of observations; so it is unusual that a LCE would extend north beyond the Exploratory Study array.

7.3.5 Type of Observations

The mix of observations was valuable – PIES, current meters, satellite altimeter, and both profiling (PALFOS) and RAFOS floats. This enabled both a 4D mapping of dynamical structures and Lagrangian tracking of water parcel trajectories. It was valuable to have 2 or more deep levels of current meter observations at several sites, especially over sloping topography, to quantify the vertical scale of bottom intensification of the currents. Now that these mean vertical scales have been mapped, it may be sufficient in future to measure deep currents at just one level at locations away from steep topography. At the mid-point of the Exploratory Study, the PIES data were collected by acoustic telemetry aboard ship while the CTD profiles were taken. The daily-processed records of variability agreed well between the telemetered data and the records recovered at the end of the observational period. In future the PIES data could be acoustically telemetered to shore in quasi-realtime.

7.4 Further Analyses

The success of the Exploratory Study observational program opens a new opportunity to analyze and understand important dynamical processes in the GOM. The measurements captured, with unique 4-dimensional space-time resolution, the coupled behavior in the upper and deep ocean

associated with LCE and strong deep eddies/waves. Moreover the observations demonstrate important vertical coupling – upper eddy developments generate deep eddies which can feed back to steer and grow and split the upper eddies. It is now understood that a numerical model that does not generate realistic deep eddies cannot hope to chart and predict the development of upper ocean currents and eddies. It is essential to the success of any numerical model to generate realistic deep eddies.

A first-order question is whether a model shows the correct deep EKE distribution relative to bathymetry and the LC. Even if one's objective is focused on just the upper ocean and accurate eddy forecasting, a model must also get the deep eddies right – whether for operational purposes or for process-modeling.

Based on analyses and evaluation described in this report, some additional "exploration" of this Exploratory Study data set could include:

- diagnostic studies of vertical motions, vertical stretching, vorticity tendency, effects of bottom topography, baroclinic/barotropic coupling;
- calculate in stream-coordinates the mean potential vorticity structure of the Loop Current and Loop Current Eddies – this tests the necessary conditions for baroclinic / barotropic instability and is useful for dynamically balanced initialization of process models;
- examine operational model(s) regarding the dynamical origin of surface features that are developed; in particular examine deep EKE values and spatial distribution; if these levels are approximately right, diagnose the associated vertical coupling processes in the presence of topography;
- examine process model(s) with these same questions regarding the deep EKE spatial distribution and dynamical diagnosis of vertical coupling processes over variable topography;
- examine near-inertial oscillations in the IES acoustic travel time data, particularly seeking to map its distribution in Eddy Sargassum, where current meters have noted a peak;
- seek to understand what process is associated with the energetic 16-day band of oscillations discovered as a common mode amongst all the bottom pressure records;
- perform a kinematic study to quantify eddy-eddy and eddy-LC interactions, both cyclonic and anticyclonic, using the available program observations in concert with coincident surface drifting buoy observations;
- develop altimeter- and PIES/altimeter-derived SSH products using optimal interpolation techniques and space/time correlation functions tuned to the SSH variability in the GOM, with the ultimate goal of combining altimeter and PIES SSH in a single data product exploiting the full sampling capabilities of the combined systems.

7.5 Recommendations for Future Deepwater Studies

The Exploratory Study improved our dynamical understanding of deepwater circulation in the GOM and allows us to refine a list of outstanding research questions.

- What regulates the northward intrusion and southward retreat of the LC and the detachment and ultimate separation of LCE?
- What processes generate and/or radiate deep energy in the GOM near and away from steep topography?
- What determines how steep topography steers, dissipates or focuses deep energy?
- Is there a feedback between deep eddies and the upper ocean; can deep eddies modulate the stability of the LC?

These questions and insights gained from the Exploratory Study motivate the design elements of future observational programs.

- Event-based or process-oriented studies that diagnose key dynamics.
- Simultaneous maps of upper and deep circulation.
- Fine horizontal resolution above steep topography.
- Current measurements at several vertical levels.
- Remote sensing for a large-scale and historical perspective.
- International cooperation for observing the GOM in a basin-wide context.
- Multi-year observational program that captures multiple LCE shedding events.
- Targeted surveys within a core array. Surveys could include glider-based high horizontal resolution surveys of a developing LCE or the interaction between the LC and a frontal eddy.

8.0 REFERENCES

Brooks, D.A. 1984. The wake of Hurricane Allen in the western Gulf of Mexico. Deep-Sea Res. 13:117-129.

Davis, R.E., J.T. Sherman, and J. Dufour. 2001. Profiling ALACEs and other advances in autonomous subsurface floats. *J. Atmos. Oceanic Tech*. 18(6):982-993.

Flierl, G.R. 1988. On the instability of geostrophic vortices. J. Fluid Mech. 197:349-388.

Hamilton, P. 1990. Deep currents in the Gulf of Mexico. *J. Phys. Oceanogr.* 20:1087-1104.

Hamilton, P. In press. Deep current variability near the Sigsbee escarpment in the Gulf of Mexico. *J. Phys. Oceanogr.*

Hamilton, P., J.J. Singer, E. Waddell, and K. Donohue. 2003. Deepwater observations in the northern Gulf of Mexico from in-situ current meters and PIES: Final report. Volume II: Technical report. U.S. Dept. of the Interior, Minerals Management Service, Gulf of Mexico OCS Region, New Orleans, LA. OCS Study MMS 2003-049. 95 pp.

Hamilton, P., T.J. Berger, J.J. Singer, E. Waddell, J.H. Churchill, R.R. Leben, T.N. Lee, and W. Sturges. 2000. DeSoto Canyon eddy intrusion study: Final report. Volume II: Technical Report. U.S. Dept of the Interior, Minerals Management Service, Gulf of Mexico OCS Region, New Orleans, LA. OCS Study MMS 2000-80. 275 pp.

Leben R.R., G.H. Born, and B.R. Engebreth. 2002. Operational altimeter data processing for mesoscale monitoring. *Marine Geodesy* 25:3-18.

Leben, R.R. 2005. Altimeter-derived Loop Current metrics. In: Sturges, W., Lugo-Fernandez, A., Schmitz, W., Jr., and Oey, L.-L., eds. *New Developments in the Circulation of the Gulf of Mexico*.

Nowlin, W.D., Jr., A.E. Jochens, S.F. DiMarco, R.O. Reid, and M.K. Howard. 2001. Deepwater physical oceanography reanalysis and synthesis of historical data: Synthesis report. U.S. Dept. of the Interior, Minerals Management Service, Gulf of Mexico OCS Region, New Orleans, LA. OCS Study MMS 2001-064. 530 pp.

Rhines, P.B. 1970. Edge-, bottom-, and Rossby waves in a rotating stratified fluid. *Geophys.Fluid Dyn.* 1:273-302.

Rossby, H.T., D. Dorson, and J. Fontaine. 1986. The RAFOS system. *J. Atmos. Oceanic Tech*. 3:672-679.

Shay, L.K. and R.L. Elsberry. 1987. Near-inertial ocean current response to Hurricane "Frederic." *J. Phys. Oceanogr.* 17:1249-1269.

The Department of the Interior Mission

As the Nation's principal conservation agency, the Department of the Interior has responsibility for most of our nationally owned public lands and natural resources. This includes fostering sound use of our land and water resources; protecting our fish, wildlife, and biological diversity; preserving the environmental and cultural values of our national parks and historical places; and providing for the enjoyment of life through outdoor recreation. The Department assesses our energy and mineral resources and works to ensure that their development is in the best interests of all our people by encouraging stewardship and citizen participation in their care. The Department also has a major responsibility for American Indian reservation communities and for people who live in island territories under U.S. administration.

The Minerals Management Service Mission

As a bureau of the Department of the Interior, the Minerals Management Service's (MMS) primary responsibilities are to manage the mineral resources located on the Nation's Outer Continental Shelf (OCS), collect revenue from the Federal OCS and onshore Federal and Indian lands, and distribute those revenues.

Moreover, in working to meet its responsibilities, the **Offshore Minerals Management Program** administers the OCS competitive leasing program and oversees the safe and environmentally sound exploration and production of our Nation's offshore natural gas, oil and other mineral resources. The MMS **Minerals Revenue Management** meets its responsibilities by ensuring the efficient, timely and accurate collection and disbursement of revenue from mineral leasing and production due to Indian tribes and allottees, States and the U.S. Treasury.

The MMS strives to fulfill its responsibilities through the general guiding principles of: (1) being responsive to the public's concerns and interests by maintaining a dialogue with all potentially affected parties and (2) carrying out its programs with an emphasis on working to enhance the quality of life for all Americans by lending MMS assistance and expertise to economic development and environmental protection.